Geophys. J. Int. (2004) **157,** 683–702 doi: 10.1111/j.1365-246X.2004.02204.x

A deep seismic transect from Hovgård Ridge to northwestern Svalbard across the continental-ocean transition: A sheared margin study

O. Ritzmann,[1,2] W. Jokat,[2] W. Czuba,[3] A. Guterch,[3] R. Mjelde[4] and Y. Nishimura[5]

[1] *Now working at: Geological Institute of the University of Oslo, The Faculty of Mathematics and Natural Sciences, Postboks 1047 Blindern, Oslo* N-0316, *Norway. E-mail: oliver.ritzmann@geo.uio.no*

[2] *Alfred Wegener Institute for Polar and Marine Research, Columbusstrasse,* 27568 *Bremerhaven, Germany. E-mail: wjokat@awi-bremerhaven.de*

[3] *Institute of Geophysics, Polish Academy of Sciences, Warsaw, Poland*

[4] *Institute of Solid Earth Physics, University of Bergen, Bergen, Norway*

[5] *Institute of Seismology and Volcanology, Hokkaido University, Sapporo, Japan*

Accepted 2003 November 17. Received 2003 September 18; in original form 2002 September 27

SUMMARY

New seismic refraction data were collected across the western Svalbard continental margin off Kongsfjorden (Ny Ålesund) during the cruise leg ARK15/2 of RV Polarstern. The use of onshore and offshore seismic receivers and a dense air-gun shot pattern provide a detailed view of the velocity structure of Svalbard's continental interior, the continent–ocean transition, and oceanic crust related to the northern Knipovich Ridge and the Molloy Ridge.

The proposed Caledonian central and western terranes of Svalbard are not distinguishable on the basis of seismic velocity structure. Below a 7 to 8 km thick Palaeozoic sedimentary cover the crystalline crust reveals a three-layer structure with seismic velocities ranging between 6.1 and 6.9 km s^{-1}. The geological suture between the terranes is imperceptible. The middle and upper crust below the Tertiary Forlandsundet graben shows low velocities. This can be related to faulting during the Early Palaeozoic movements between Svalbard and northern Greenland, followed by the continental break-up. Moreover, a sedimentary Palaeozoic core is may be buried below the Forlandsundet graben.

The continent–ocean transition can be classified as an obliquely sheared (transform) continental margin. The Moho dips with an angle of 45° eastwards at the continent–ocean transition that exhibits higher seismic velocities of more than 7.2 km s^{-1}on the continental side. The sheared margin evolution is linked to the Spitsbergen Transform Fault, today located north of the Molloy Ridge spreading segment. During a later evolutionary stage the Molloy Ridge passed the continental margin. The separating boundary between continental and oceanic crust off northwestern Svalbard is today part of the inactive Spitsbergen Fracture Zone. The high seismic velocities at the continent–ocean boundary can be interpreted as minor mantle-derived intrusions, probably induced by interaction of the passing spreading ridge during the sheared margin evolution.

The oceanic crust generated at the Knipovich Ridge and the Molloy Ridge is thin (2 to 4 km), compared to the global mean, and is thinner as previously observed. The oceanic crust is characterized by the absence of oceanic layer 3. These observations can be ascribed to conductive cooling of the ascending mantle as a result of the extremely low divergence rate.

The underlying mantle is slightly serpentinized below the Knipovich Ridge segment, reflected by low seismic velocities of ∼7.7 km s^{-1}. A thicker sequence of syn- and post-rift sediments and sedimentary rocks are observed on the Molloy Ridge oceanic segment, which most likely results from greater subsidence relative to the Knipovich Ridge segment.

Key words: continental margins, crustal structure, fracture zone, refraction seismology, Svalbard.

INTRODUCTION

The Palaeozoic to Cenozoic tectonic history of western Svalbard is revealed onshore along a stretch of outcrops that form an area 150 km wide and is morphologically intersected by large fjords (i.e. Kongsfjorden and Isfjorden; Fig. 1). This coastal strip and the adjacent continental margin were affected by various tectonic events, which are mostly associated with strike-slip movements. The

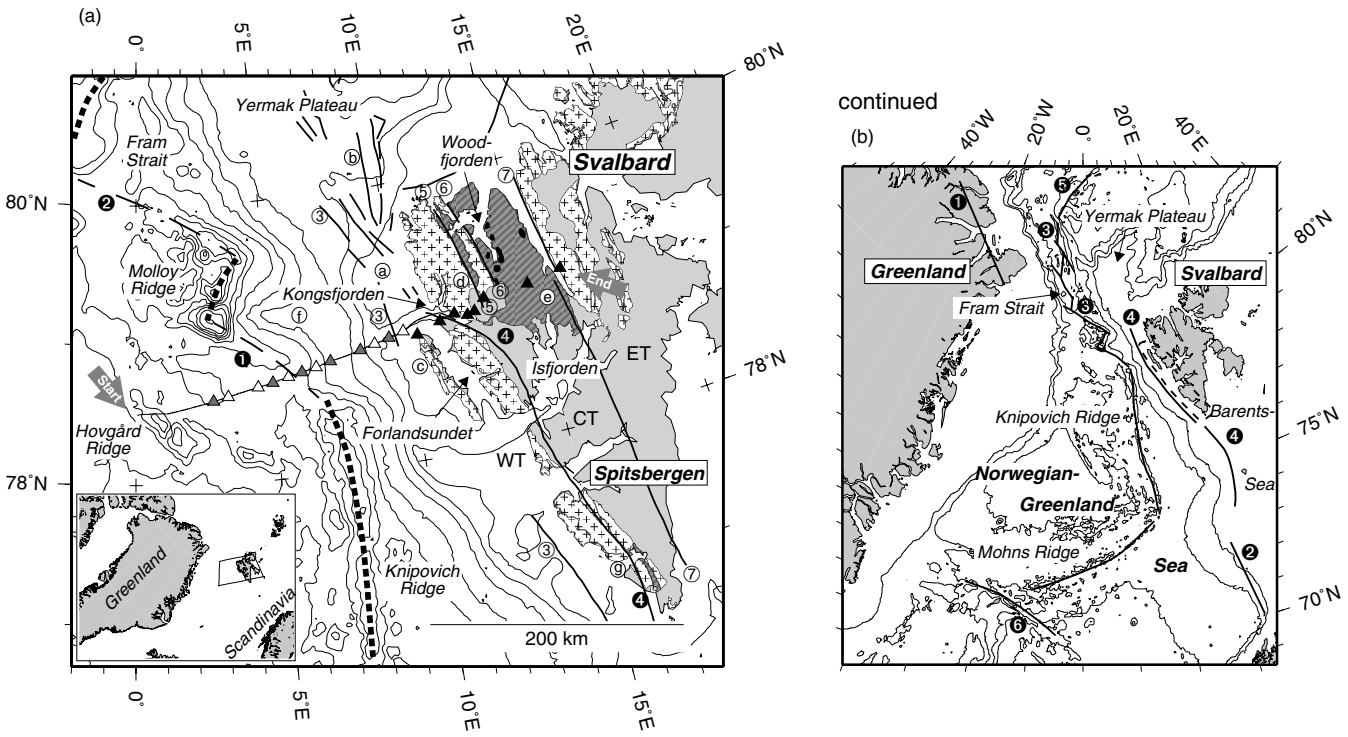

Figure 1. (Location of profile AWI-99400.) (a) Location of seismic refraction profile AWI-99400. Insert: location in the North Atlantic. The profile track is marked by a thin black line, RefTek stations (black), OBH stations (grey) and OBS stations (white) by triangles. The cross marks indicate pre-Devonian basement outcrops (after Harland 1997a simplified geological map). Devonian sedimentary rocks are coloured dark grey (dash pattern). Local outcrops of Quaternary volcanics in the Woodfjorden area are plotted as black polygons. Thick black lines are major faults offshore (dashed) and onshore (solid): (1) Molloy Transform Fault, (2) Spitsbergen Transform Fault, (3) Hornsund Lineament, (4) Kongsfjorden–Hansbreen Fault Zone, (5) Raudfjorden Fault, (6) Breibogen Fault, (7) Billefjorden fault. Spreading ridges are marked by a thick dotted line. Geographic locations used in the text: (a) Sjubrebanken, (b) Danskøya Basin, (c) Prins Karls Forland, (d) Albert I Land, (e) Andrée Land, (f) Vestnesa, (g) Hornsund. Note, sinistral strike-slip faults (4) and (7) are proposed to subdivide Svalbard into the western, central and eastern terrane (WT, CT and ET). Plate boundary after Boebel (2000). Bathymetry: IBCAO (500 m contour interval +200 m contour; Jakobsson *et al.* 2000). (b) Tectonic structures in the North Atlantic region. The thick dotted line indicates the approximate position of the west Spitsbergen fold belt. (1) Trolle-Land Fault Zone, (2) Senja Fracture Zone, (3) mid-ocean ridges and transforms within the Fram strait according to Boebel (2000), (4) Hornsund Lineament and Bjørnøya-Sørkapp Fault, (5) Gakkel Ridge, (6) Jan Mayen Fracture Zone.

earliest of these was the sinistral merging of Palaeozoic basement terrane (Harland & Wright 1979; Harland 1997b). Later, in the Early Cenozoic, the west Spitsbergen orogeny (e.g. Dallmann *et al.* 1993; Harland 1997a) took place. The latest step in the tectonic history was the dextral transtensional rifting and breakup between Svalbard and northeast Greenland (Eldholm *et al.* 1987). The present-day spreading axes of the Knipovich Ridge and the Molloy Ridge within the Fram strait are situated close to the margin, which might enhance magmatic interactions from the ridges to the continental crust.

As a result of the absence of detailed deep seismic transects across the archipelago, large gaps still exist in the knowledge about the deeper crustal composition of northwestern Svalbard and the adjacent western continental margin. Early experiments explored this region only locally (e.g. Guterch *et al.* 1978; Myhre & Eldholm 1988; Faleide *et al.* 1991; Sellevoll *et al.* 1991). A number of modern seismic refraction experiments reveal the detailed seismic structure along the southern Svalbard—western Barents sea margin further south, and show a clear segmentation of the eastern North Atlantic margin into rifted and sheared continental margins (e.g. Breivik *et al.* 1999, 2003) (Ritzmann *et al.*, 2002). Moreover, accompanied local volcanic activity is achieved along the margin (Eldholm *et al.* 1987).

This contribution provides new detailed background information on the crustal structure of the continental margin of northwestern Svalbard at the latitude of the Kongsfjorden (Fig. 1a). The presented seismic profile extends the number of observations along the North Atlantic margin further to the north and completes knowledge about North Atlantic margin segmentation. We base our study on a seismic refraction experiment between Hovgård ridge and the Billefjorden Fault Zone in northwestern Svalbard (Fig. 1) with an integrated analysis of gravity data. This experiment was carried out by the Alfred Wegener Institute for Polar and Marine Research (Bremerhaven) in cooperation with Polish, Japanese and Norwegian scientists from 1999 August to September with the German Icebreaker RV Polarstern.

CALEDONIAN GEOLOGY

The Svalbard archipelago (Figs 1a and b) is supposed to consist of three distinct terranes, that are bounded by major discontinuities (e.g. the Kongsfjorden–Hansbreen Fault Zone; Harland & Wright 1979). These terrane merged during the early Silurian–Devonian closure of the Iapetus ocean by sinistral transform movements. Recent compilations of Svalbard's geology (e.g. Harland 1997b) support this hypothesis, although other authors continue to treat the Pre-Devonian of Svalbard as one province (e.g. Manby & Lyberis 1992). The central terrane covers most of the northwestern part of Spitsbergen, the main island of the archipelago. The central terrane itself is separated into at least three subterranes (or basement provinces) that also docked in Silurian/Devonian times by sinistral

movements along transform faults (e.g. Breibogen Fault; Friend *et al.* 1997). Primarily these faults controlled the Devonian sedimentation history of northwestern Svalbard (Harland 1997b) between the Breibogen Fault and the Billefjorden Fault zone (Fig. 1a). Further Devonian deposits are found along the Raudfjorden Fault zone in the Woodfjorden region. Here, narrow half-grabens occur along the fault, suggesting that simple shear tectonics occurred in Palaeozoic time. This results in extension and proposed large-scale detachment tectonics (Friend *et al.* 1997). Locally, Devonian sedimentary rocks are also preserved within the west Spitsbergen fold belt . (Hornsund; Fig. 1b Steel *et al.* 1985).

TERTIARY BREAK-UP AND WESTERN SPITSBERGEN FOLD BELT

Tertiary break-up of Svalbard and northern Greenland was initiated by the beginning of seafloor spreading at the Mohns Ridge in the Norwegian–Greenland sea (Fig. 1b) at ∼chron 25 (∼57 Ma; Talwani & Eldholm 1977; Eldholm *et al.*1987). Between Svalbard and Greenland shear movements took place along the Trolle Land-Senja Fault Zone (Håkansson & Pedersen 1982; Eldholm *et al.* 1987), while later an eastward migration to the Hornsund Lineament (Eiken & Austegard 1987) occurred. Crane *et al.* (1991) term this broad shear region the Spitsbergen shear zone, which also includes the Bjørnøya-Sørkapp Fault (Fig. 1b) connecting the juvenile Senja transform margin to the Hornsund Lineament. The west Spitsbergen fold belt, today localized within a 50 km wide region along the western coast of Spitsbergen (Fig. 1a) evolved mainly during the early Tertiary. The prevailing compressional structure of the belt suggests that convergent tectonics dominated the fold and thrust development, despite the fact that local geological record causes difficulties to simple convergent models. Recent models (based on structural geological record) therefore suggest two decoupled tectonic regimes, i.e. coeval offshore strike-slip movements and convergent folding of the belt (Dallmann *et al.* 1993). The Late Eocene to Oligocene evolution of the western Svalbard region is supposed to comprise transtensional movements also, because subsidence of the Forlandsundet graben is observed (e.g. Steel *et al.* 1985; Dallmann *et al.* 1993).

Between chrons 13 and 5 (36 to 9.5 Ma) the very slow spreading Knipovich Ridge ($<$10 mm yr^{-1}; Eldholm *et al.* 1990) is supposed to have propagated northward into the shear zone, resulting in extremely asymmetric spreading (Crane *et al.* 1991, 2001; Eldholm *et al.* 1990). Further north the precise plate boundary between Svalbard and Greenland within the Fram strait (Fig. 1b) was defined by Boebel (2000) by modelling airborne gravity data. The associated reconstruction, based on the poles of rotation of Srivastava & Tapscott (1986) suggests the onset of seafloor spreading at Molloy Ridge in the Early Miocene (20 Ma). Further north, two ancient ridge–transform pairs (Fig. 1b) balanced the gradual opening of the Fram strait oceanic gateway since chron 5 (12 to 9.5 Ma). The seafloor spreading of these ridges within the Fram strait is expected to be oblique, as observed for the Knipovich Ridge (Eldholm *et al.* 1990; Boebel 2000).

THE DEEPER STRUCTURE OF SVALBARD AND THE ADJACENT OCEANIC PROVINCE

Offshore seismic surveys have been conducted for the past 30 yr, and comprise seismic reflection experiments and expanding spread profiling (Eiken & Austegard 1987; Myhre & Eldholm 1988; Faleide *et al.* 1991; Eiken 1993; Eiken & Hinz 1993) or larger refraction experiments using a small amount of seismic receivers and shots (Guterch *et al.* 1978; Sellevoll *et al.* 1991; Czuba *et al.* 1999). A first detailed crustal study along the northwestern shoreline and the southern Yermak Plateau was carried out by RV Polarstern (Jokat *et al.* 2000; Ritzmann 2003; Ritzmann & Jokat 2003).

Guterch *et al.* (1978) and Sellevoll *et al.* (1991) defined the crustal thickness below central Svalbard to be from 36 to 37 km and below the Forlandsundet from 26 to 27 km. Ritzmann & Jokat (2003) found similar crustal thicknesses of 28 km along the northwestern coast of Svalbard north of Prins Karls Forland. Sellevoll *et al.* (1991) and Czuba *et al.* (1999) report anomalously high seismic velocities at the crust–mantle boundary, assuming a transitional character of the Moho. This observation is not confirmed by Ritzmann & Jokat (2003), who assume a first-order crust–mantle discontinuity. The petrological constitution of the central terrane is derived from xenolith studies within the Woodfjorden volcanics (Fig. 1). Amundsen *et al.* (1987) define a three-layered structure of gneisses, granulites and intrusive granulites (mantle pyroxenites and lherzolites) for northwestern Svalbard that supports the seismic model of Chan & Mitchell (1982) and Ritzmann & Jokat (2003). Subdivision into terranes after Harland & Wright (1979) based on seismic velocity discrimination appears doubtful as a result of the probable absence of remarkable velocity diversity across the terrane borders.

Crustal models across the western continent–ocean transition were also deduced by velocity information of expanding spread profiles and gravity data (Sundvor & Austegard 1990). Off Isfjorden a high velocity/density body is supposed to extend up to 2 km below the seafloor (Sundvor & Austegard 1990). Published thicknesses of the oceanic crust associated to the Knipovich Ridge range between 8 and 12 km (Sundvor & Austegard 1990; Czuba *et al.* 1999). Recently, a much lower thickness was observed at the latitude of the Van Mijenfjorden (south of Isfjorden; Fig. 1; Ritzmann *et al.*2002). Here, only 2 to 4 km thick oceanic crust are confirmed on either side of the Knipovich Ridge. The actual transition of continental and oceanic crust is mainly located using seismic reflection data. Up to 79°N the boundary is thought to be located at the Hornsund Lineament (Myhre & Eldholm 1988; Sundvor & Austegard 1990). It comprises a series of blocks downfaulted to the west, while on northern Sjubrebanken it separates into two distinct NNW-trending blocks (Myhre & Eldholm 1988). The sedimentary structure off Svalbard is mapped by several seismic reflection lines (Eiken 1994). According to the sedimentary distribution map of Austegard & Sundvor (1991), thicknesses vary between 1 and 3 km along the western Svalbard margin east of the Knipovich Ridge. Sedimentary deposits show a prominent depocentre at Vestnesa (up to 5 km), that is also a prominent feature in bathymetry (Fig. 1a). The sedimentary structure of the offshore Tertiary graben, e.g. Forlandsundet graben, was characterized by the work of Eiken & Austegard (1987). They conclude that structurally these graben are relatively small, but deep basins (up to 5 km), which terminate north of Prins Karls Forland, however, it is not clear whether or not these grabens are related to strike-slip movements; a simple extension model can explain the observed structures. Later, Eiken (1993) proposed that an up to 10 km wide graben on northern Sjubrebanken to be similar to the Forlandsundet graben structure.

NEW GEOPHYSICAL DATA

Seismic data acquisition

Seismic measurements along profile AWI-99400 were performed with the German icebreaker RV Polarstern during cruise leg

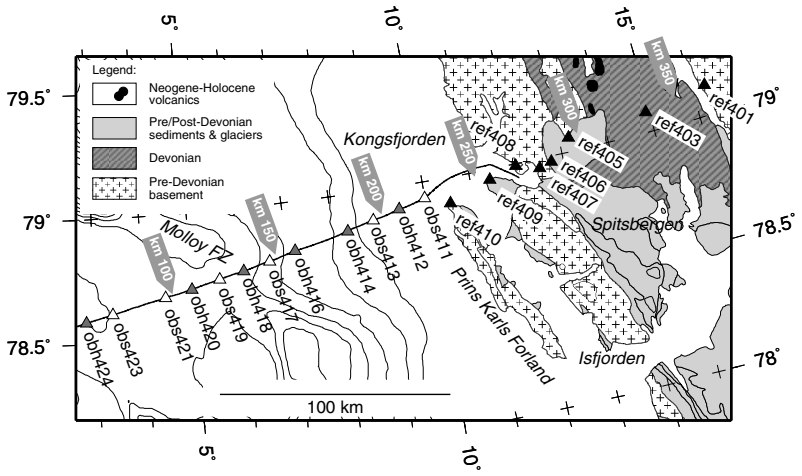

Figure 2. Locations of receiver stations: detailed map of profile AWI-99400 and locations of receivers. The profile track in the main figure is marked by a thin black line, triangles as for Fig. 1. Bathymetry: IBCAO (Jakobsson *et al.* 2000).

ARK15/2 (Jokat *et al.* 2000). Two large volume air-guns with a total volume of 92 l produced the acoustic energy and were fired every minute (approximate distance of 170 m). In total the 1628 air-gun shots extend from 0°to 12°E from Hovgård Ridge to Kongsfjorden along a profile distance of 250 km (Figs 1a and 2). Additionally the Polish ship El Tanin participated with five TNT shots with a charge of 50 kg between 8.5°and 9.5°E. Onshore, eight RefTek seismometer stations, each equipped with 18 single-coil geophones (4.5 Hz; vertical component) were used to record seismic energy. The easternmost station (ref401) was installed at 16.3°E, which results in an overall length of profile AWI-99400 of 360 km. The spacing of the onshore receiver stations range from 5 to 35 km, and their deployment altitudes vary from 10 to 900 m. West of Prins Karls Forland seven ocean-bottom hydrophone and eight three-component seismometer systems (4.5 Hz geophones, gimbal mechanism) were deployed in water depths of 200 to 2500 m BSL. A receiver spacing of approximately 12 km was chosen for ocean-bottom instruments. Failures of the stations obs425/obs415 and obh422 result in two larger gaps of 24 km along the profile (3°E and 7.7°E; Fig. 2). The profile AWI-99400 is unreversed west of station obh424 (2.8°E) as well as east of ref408 (12°E; Fig. 2).

Characteristics of seismic refraction data

Figs 3(a)–(h)show eight representative record sections out of the 20 successful registrations onshore and offshore. The sections illustrate the main characteristics of the observed crustal velocity distribution. The data are filtered with a bandpass filter passing frequencies between 5 and 17 Hz. A 1 s-automatic gain control (AGC) was applied for the evaluation and analysis of seismic refraction data. The data quality of the RefTek (Dallas, TX, USA) seismometers is in general good. Maximum distances of recorded arrivals are up to 220 km (P_n arrivals). Mostly, a low signal-to-noise ratio is compensated by the dense shot spacing yielding a good phase correlation.

Offshore, the ocean-bottom seismometer systems provide higher quality data than the neighbouring hydrophone systems. Some hydrophone systems reveal extremely poor quality, so that data were ignored during picking and ray tracing (obh414 and obh416). Table 1 lists the phase indexes used in the following paragraph.

First arrivals on seismic sections recorded by receivers east of Kongsfjorden at near distances (20 to 30 km offset) are upper crustal phases penetrating pre-Devonian basement rocks with *P*-wave velocities of 5.4 to 6.2 km s^{-1}(Figs 3a and b; P_{uc}). Direct constraints on the seismic velocities of the (lower) Devonian sedimentary rocks further east is only given by station ref403 (6.2 km s^{-1}). At greater offsets, weak *P*-wave arrivals point to lower velocity gradients in the deeper crust (Figs 3a and b; P_{mc}). Weak lower crustal reflective energy along the eastern part of the profile is observed on several recordings (Fig. 3a; $P_{lc}P$). As a result of the general reverberation of the source signal it is difficult to distinguish between a single reflection or a broader reflective lower crustal zone. The P_mP reflections mark the crust–mantle boundary on several onshore recordings (Figs 3a and b; P_mP). Recordings from stations near Kongsfjorden are characterized by $P_{uc/mc}$ -phase undulations, i.e. the increase/decrease of apparent seismic velocity pertaining to lateral velocity variations in the middle crust at 220 km (Fig. 3c). The same effect is also observed on the reversed sections (e.g. Fig. 3e; P_{gm}). Here, seismic velocities of 7.0 km s^{-1}are found at near offsets, while they are lower towards the east (6.0 km s^{-1}). Lower crustal reflections are slightly stronger along this part of the profile (Figs 3d and e; $P_{lc}P$). Seismic data recorded off Prins Karls Forland provide further reliable velocity information of the Tertiary sedimentary section westwards to the Molloy Transform Fault (Figs 3d–f; P_{cb}) of 2.2 to 3.5 km s^{-1}. The seismic structure on both sides of the Molloy Transform Fault (120 km) differs, i.e. to the east crustal P_g arrivals appear with lower seismic velocity than to west (Fig. 3g P_{go}). Further, the arrival times of P_n phases are up to 2 s delayed suggesting a thicker sedimentary cover and/or a deeper crust-mantle boundary. Mantle phases recorded by more distant stations, e.g. obs423, show characteristic phase undulations at the position of Molloy Transform Fault (Fig. 3h; P_n). P_n phases reveal lower amplitudes compared to P_g phases most probably as a result of low vertical velocity gradients. Seismic velocities of mantle phases at the western edge of the profile are remarkably low and we assume a deepening crust–mantle topography towards the Hovgård Ridge, whose shallower bathymetry causes phase undulations of mantle arrivals (Fig. 3h; P_n).

Generally, the observed seismic energy is extremely low for deeper crustal phases at absolute profile distances of 150 to 180 km, i.e. the signal-to-noise ratio decreases to values below 1. This zone is roughly at the Hornsund Lineament, the supposed continent–ocean transition (Fig. 1). It seems that rock properties along this transition

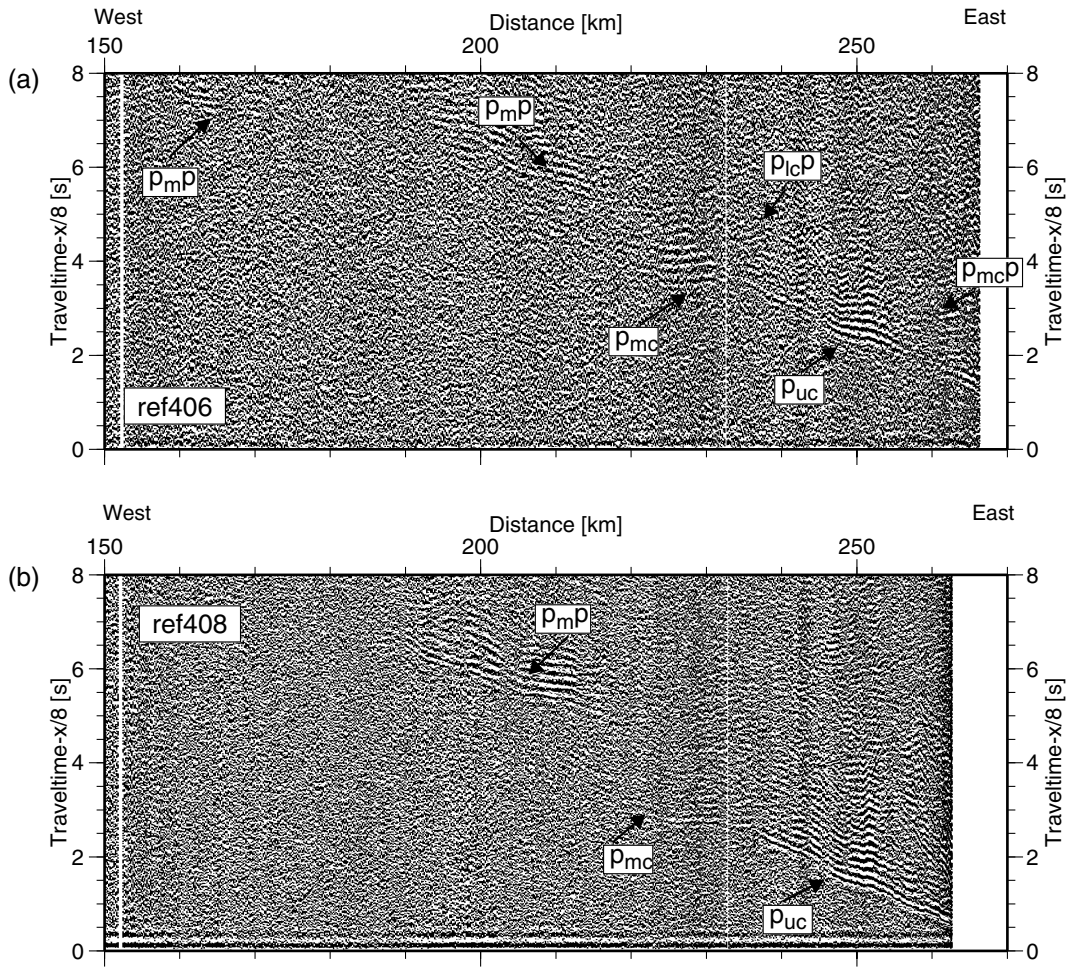

Figure 3. Seismic refraction data examples: record sections of onshore and offshore receivers. (a)–(c): RefTek seismometer systems (ref). (d)–(h): ocean-bottom seismometer/hydrophone systems (vertical component; obs/obh).

are responsible for the damping/scattering of seismic energy. Despite this, the seismic velocities for the upper mantle are well resolved as a result of P_n-phase arrivals observed on either side of this geological complex zone.

2-D kinematic ray tracing

Modelling of the seismic refraction data was performed using the ray-tracing rayinvr software of Zelt & Smith (1992).

(i) Traveltimes of reflected and refracted phases were picked on each record section. 1-D velocity profiles were calculated and gathered to a 2-D section along the profile track.

(ii) The derived model was used as the initial source for 2-D kinematic ray tracing using a forward modelling technique. The modelling took place layer by layer and velocity-depth nodes were held constant when the next, deeper layer was modelled. To further enhance the fit of observed traveltimes additional velocity-depth nodes were implemented. More attention was paid to matching the slope and shape of the observed traveltimes than reducing the RMS-traveltime residual calculated by the rayinvr programme.

(iii) Once the model provided a reasonable overall fit of observed and calculated traveltimes, the traveltimes of all possible phases were calculated. Thus, it was possible to search for additional information on seismic sections, such as low-amplitude arrivals as a result of low-velocity gradients. This information was added to the existing traveltime observations. The final set of traveltime picks (about 2500) and modelled traveltimes are shown in Fig. 4 for each of the analysed seismic stations. The appropriate ray traces for the modelled layers are shown in Fig. 5.

(iv) Where possible, the final model was improved by two runs of the application of the inversion algorithm of rayinvr to enhance the match between calculated and observed traveltimes. This procedure was only possible for profile sections without any steep layer boundaries, i.e. the eastern continental as well as the western oceanic section of the profile, but not at the transitional section between obh412 and obs417 (Figs 1a and 2).

The final velocity model

The final modelling result after ray tracing is shown in Fig. 6 for the sedimentary section between 20 and 260 km, and Fig. 7 for the entire crustal section. Generally, the oceanic section (0 to 180 km) fits well the observed traveltimes using a one-layer constant gradient model with an overlying sedimentary section. Further east, the observed traveltimes of stations on the continental crust were modelled by a three-layer model.

Cenozoic sedimentary section

The thickness of the Cenozoic sedimentary cover, which overlays partly oceanic, transitional and continental crust varies from 1 km

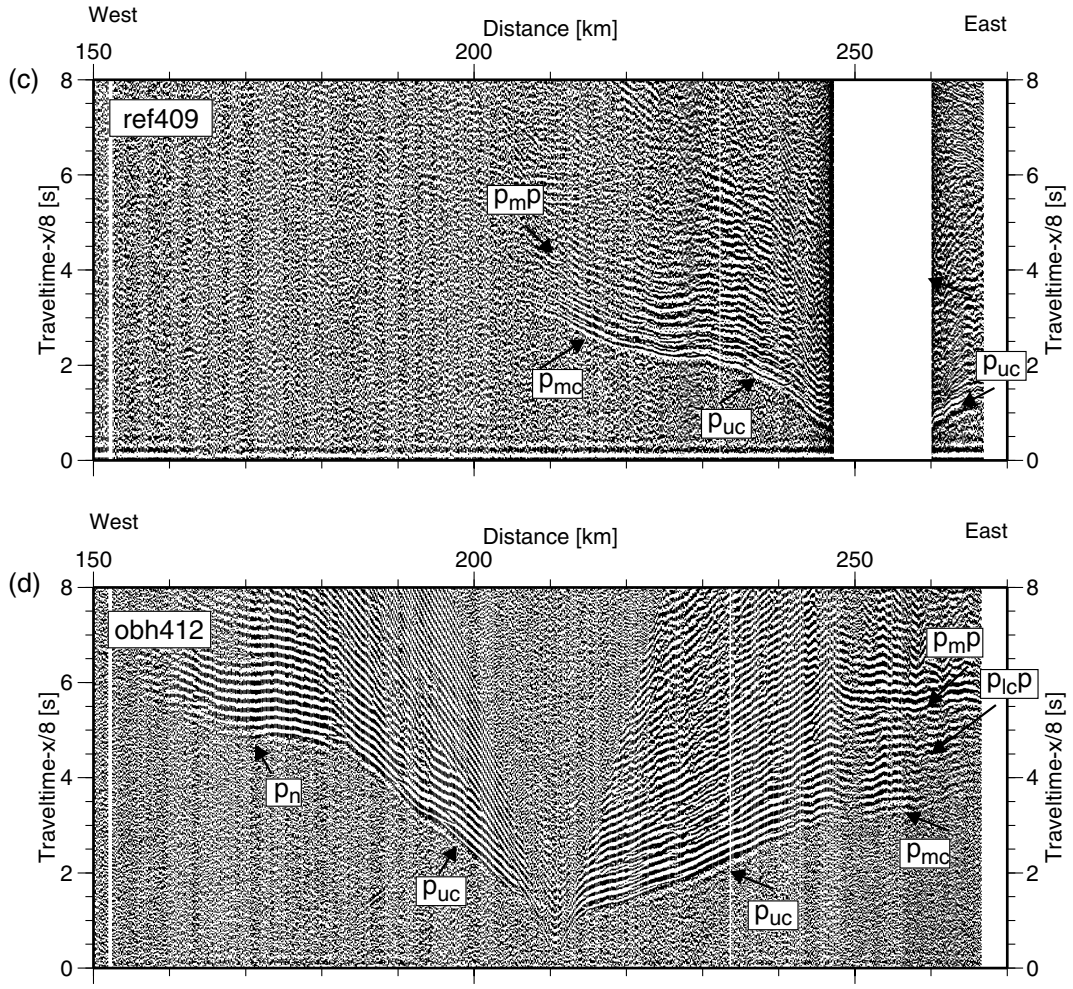

Figure 3. *Continued.*

(close to the Hovgård Ridge) to approximately 6 km east of the Molloy Transform Fault (Fig. 6). Seismic velocities range from 2.2 km s^{-1}at the top to 3.8 km s^{-1}close to the basement at the continental slope. According to Eiken (1993), Eiken & Hinz (1993) and Geissler (2001) the seismic velocities of the uppermost sequences off northwestern Svalbard are in general lower than observed here (∼1.7 km s^{-1}). This effect may be related to the applied low-frequency energy source for our profile, which limits the vertical resolution. To the west, sedimentary thickness does not exceed 2.3 km and the seismic velocities of the lower sections range from 2.3 to 2.7 km s^{-1}at maximum. A remarkable decrease of seismic velocity occurs at 90 km, where the upper sedimentary strata show seismic velocities of 1.8 km s^{-1}. Sedimentary rocks of the Tertiary Forlandsundet graben at 240 km (Fig. 6) exhibit high velocities of 3.5 to 4.1 km s^{-1}, which mark the highest values for Tertiary sedimentary rocks along the entire profile.

Eastern continental section and the continent–ocean transitio

The final velocity model of the eastern continental section of profile AWI-99400 consists of three units. The upper unit, with velocities between 5.4 and 6.2 km s^{-1}reveals a thickness of 10 km in the east, while it thins to the west to approximately 5 km over the flanks of an updoming structure north of the Forlandsundet graben (Fig. 7). The underlying unit has velocity from 6.4 to 6.6 km s^{-1}at depths of 20 to 23 km between 250 and 360 km. In the upper parts of a zone of lower velocity beneath Forlandsundet graben, seismic velocities range between 5.8 and 6.0 km s^{-1}. This vertical feature has a width of 20 to 30 km along the profile and a maximum depth of 18 km, where the decreased velocity is 6.4 km s^{-1}. The best fit of observed and modelled traveltimes (from stations ref409 and obs413; Fig. 3c and e) was achieved by implementing this low-velocity structure in the model. The fit of traveltimes decreases using velocity models characterized only by dip of individual layer boundaries (that can also cause undulations in refracted phases).

The lower unit of the eastern continental section is characterized by velocities of 6.7 to 6.9 km $s^{-1}$and thins slightly westwards from 9 to 5 km. This unit is not directly constrained by refraction arrivals. Indications for lower crustal reflections are the basis of this individual unit whose vertical velocity gradient was similarly low to that in the middle crustal layer above. Thus, the entire crustal thickness (excluding Cenozoic sediments) along the section decreases from 32 km in the east to 14 km at 190 km. Here, at the continent–ocean transition (180 to 200 km) velocities are slightly elevated to 6.8–7.2 km s^{-1}(at depths of 10 to 20 km) compared to the section east of 250 km. The transition itself is marked by an abrupt decrease of Moho depth towards the west. The remarkably seaward termination of continental crust and elevated seismic velocities are well constrained by seismic recordings. As shown is Fig. 8, the lower crustal reflectivity ($P_{lc}P$ phases) and the Moho are evidenced up to 175 km.

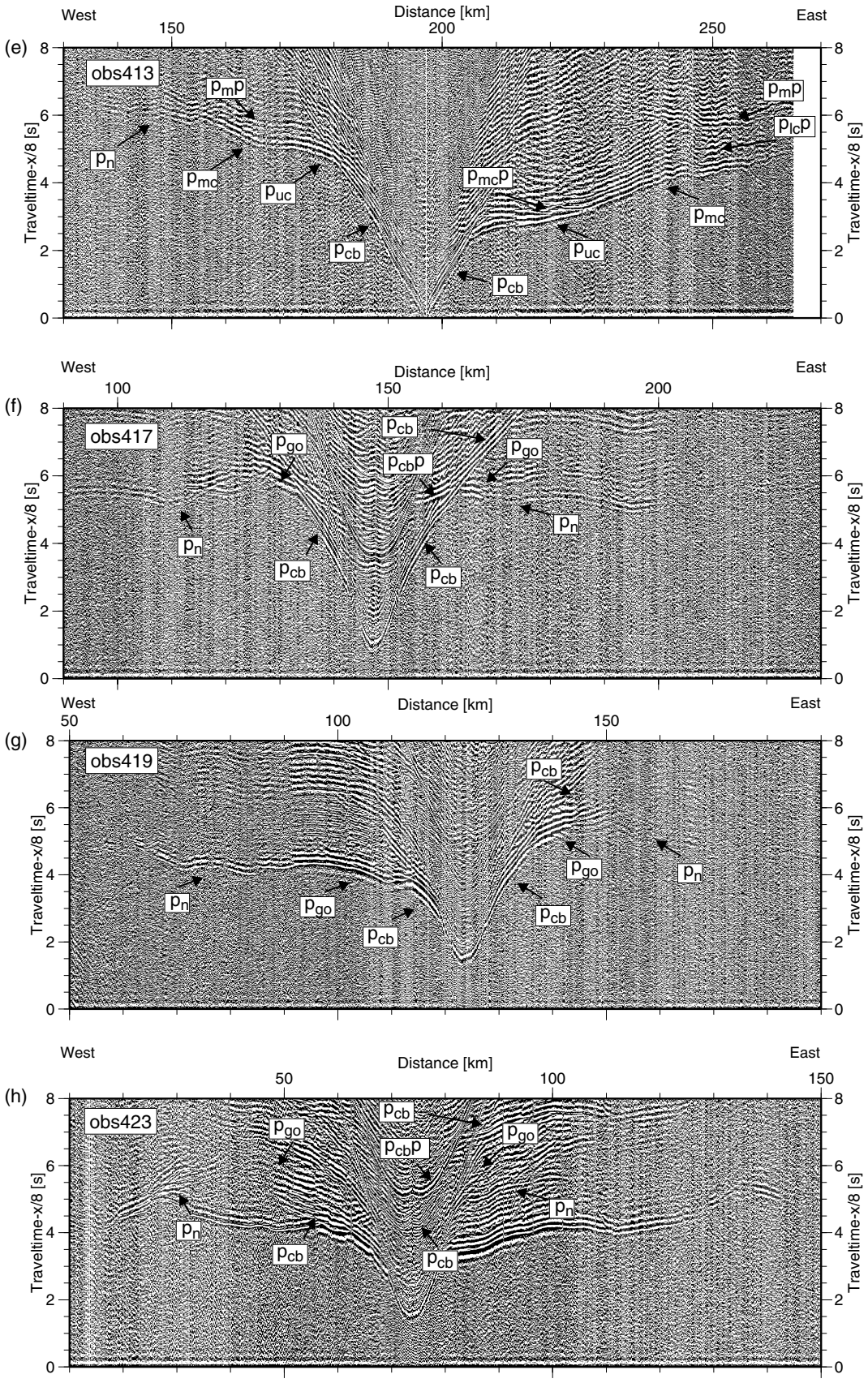

Figure 3. *Continue.*

Table 1. Phase indexes used in text and figures (*P*-wave only).

	Phase index	Type, penetrating layer
Continental	P_{pb}	Refracted wave, Palaeozoic sedimentary basin
	P_{uc}	Refracted wave, continental upper crust
	P_{mc}	Refracted wave, continental middle crust
	P_n	Refracted wave, upper mantle
	$P_{mc}P$	Reflected wave, top middle continental crust
	$P_{lc}P$	Reflected wave, top lower continental crust
	P_mP	Reflected wave, Moho
Oceanic	P_{cb}	Refracted wave, offshore Cenozoic sedimentary basin
	$P_{cb}P$	Reflected wave, top oceanic basement
	P_{go}	Refracted wave, oceanic crust
	P_n	Refracted wave, upper-mantle

Seismic stations located between 190 and 220 km cover the easternmost section of continental crust very well. The seismic record of stations located slightly further to the west, west of 175 km, reveal a completely different seismic structure, i.e. thinned oceanic crust (see below).

Western oceanic section and Hovgård Ridge

The igneous crust of the oceanic section of the profile (50 to 180 km) is mostly thin, ranging from approximately 2 km west of Molloy Transform Fault to 4.5 km to the east underlying a thick portion of Cenozoic sedimentary layers (Fig. 7). Seismic velocities east of Molloy Transform Fault range from 5.3–5.4 km s^{-1}at the top to 5.5–5.8 km s^{-1}at deeper levels. The transform itself marks a transition to higher velocities in the crustal section. West of the transform fault velocities of 5.8–6.1 km $s^{-1}$are observed for the upper parts, while downwards they increase to approximately 6.3–6.6 km s^{-1}at the crust–mantle boundary. At the Hovgård Ridge (0 to 40 km) the crustal thickness increases to 11.5 km. Stations obs423 (Fig. 3h) and obh424 give a reliable view of a change in seismic velocities for upper basement at 80 km. Velocities are markedly lower west of this point (3.3 to 3.6 km s^{-1}). Downwards, velocities increase to approximately 6.0 km s^{-1}at the crust–mantle boundary. Because the profile is unreversed west of obh424 (Fig. 2) the seismic velocity structure of the Hovgård Ridge remains speculative. West of the stations obs423/obh424 the velocity–depth function was held fixed, merely the basement and crust–mantle topography were altered to fit traveltimes.

Upper mantle

Upper-mantle seismic velocities are highest below the eastern continental section of the profile: 8.0 to 8.1 km $s^{-1}$are modelled at profile distances of km 190 to 360. Towards the Molloy Transform Fault velocities decrease to 7.9 km s^{-1}west of the steep rise of the crust–mantle boundary at 175 km. Directly at the Molloy Transform Fault low seismic velocities between 7.6 and 7.7 km $s^{-1}$are modelled (65 to 120 km). Seismic velocities of the upper mantle increase again to 8.0 km s^{-1}below Hovgård Ridge.

Quality of the final velocity model

The quality of the final velocity model is illustrated by the following methods:

(i) RMS misfit, χ^2 values and resolution after the methods of Zelt & Smith (1992) derive a standardized mathematical expression of traveltime fit in relation to observations and model parametrization.

(ii) Further empirical tests on the final velocity model were conducted in order to provide the uncertainties of modelled depth and velocity range.

RMS misfit and χ^2 after Zelt & Smith (1992)

First constraints on the certainty of the final velocity model is given by the RMS misfit and χ^2-normalized misfit parameter provided by rayinvr (Zelt & Smith 1992). These parameters were controlled during the entire modelling procedure. Table 2 lists the derived values for each phase based on the final velocity model. The calculated RMS misfits are within the range of assigned errors of the traveltime picks. The deeper the seismic phase penetrates the subsurface the better RMS misfit is achieved. We relate this to the generally complex surface geology that results in lateral seismic velocity variations.

In addition to this, χ^2 values derive further support: A value of 1 indicates that the picked traveltimes are fitted within their assigned errors in relation to parametrization of the velocity model. The insertion of additional node points derives the decrease of χ^2 (Zelt & Smith 1992). Nevertheless, a complex geological structure requires further parametrization, e.g. during reproduction of steep vertical geological units or strong lateral seismic velocity variations. Instead, a non-linear experimental setup during the seismic refraction experiment results in increased χ^2 values. This applies specially for the deployed onshore seismic receiver stations. Here, the combined onshore and offshore setup has a particular effect on the χ^2 calculation. On the basis of this discussion we regard the derived values as acceptable because the majority lie between 0.78 and 1.78. Merely, the values for the onshore Palaeozoic basin (only sparse information) and the offshore Cenozoic sedimentary wedge show higher values. The overall RMS misfit and χ^2 value for the entire model are 0.21 and 1.46, respectively.

Resolution after Zelt & Smith (1992)

The resolution of the crustal model was assessed using the inversion method of Zelt & Smith (1992). The relative number of rays which determine the parametrization of the velocity model (i.e. velocity and boundary nodes) are the principle of this quantitative approach. In this case we calculated only the numerical resolution of velocity nodes.

Fig. 9(a) summarizes the resulting resolution for the sedimentary section. Generally, values greater than 0.5 are considered to be well resolved (Zelt & Smith 1992). Due to the large number of diving waves the upper sedimentary section between 100 to 200 km is well resolved. To the west the lack of reversed shots is responsible for resolution values near zero for the sedimentary section, which are not shown in Fig. 9(a).

The eastern continental section of the profile shows a very uneven lateral and vertical distribution of resolution values (Fig. 9b). From 180 to 250 km of the upper unit are well resolved showing values of 0.7 to 0.9. Downwards and towards the east resolution decreases to 0.2 to 0.4. The same is true for the middle unit (10 to 20 km depth), although the low-velocity zone between 220 and 250 km is well resolved. The lower levels are poorly constrained with values of 0.2 to 0.5. Modelled rays of wide-angle reflections increase the resolution to 0.6 in the middle unit further to the east (320 km). The lower unit above the crust–mantle boundary is better constrained,

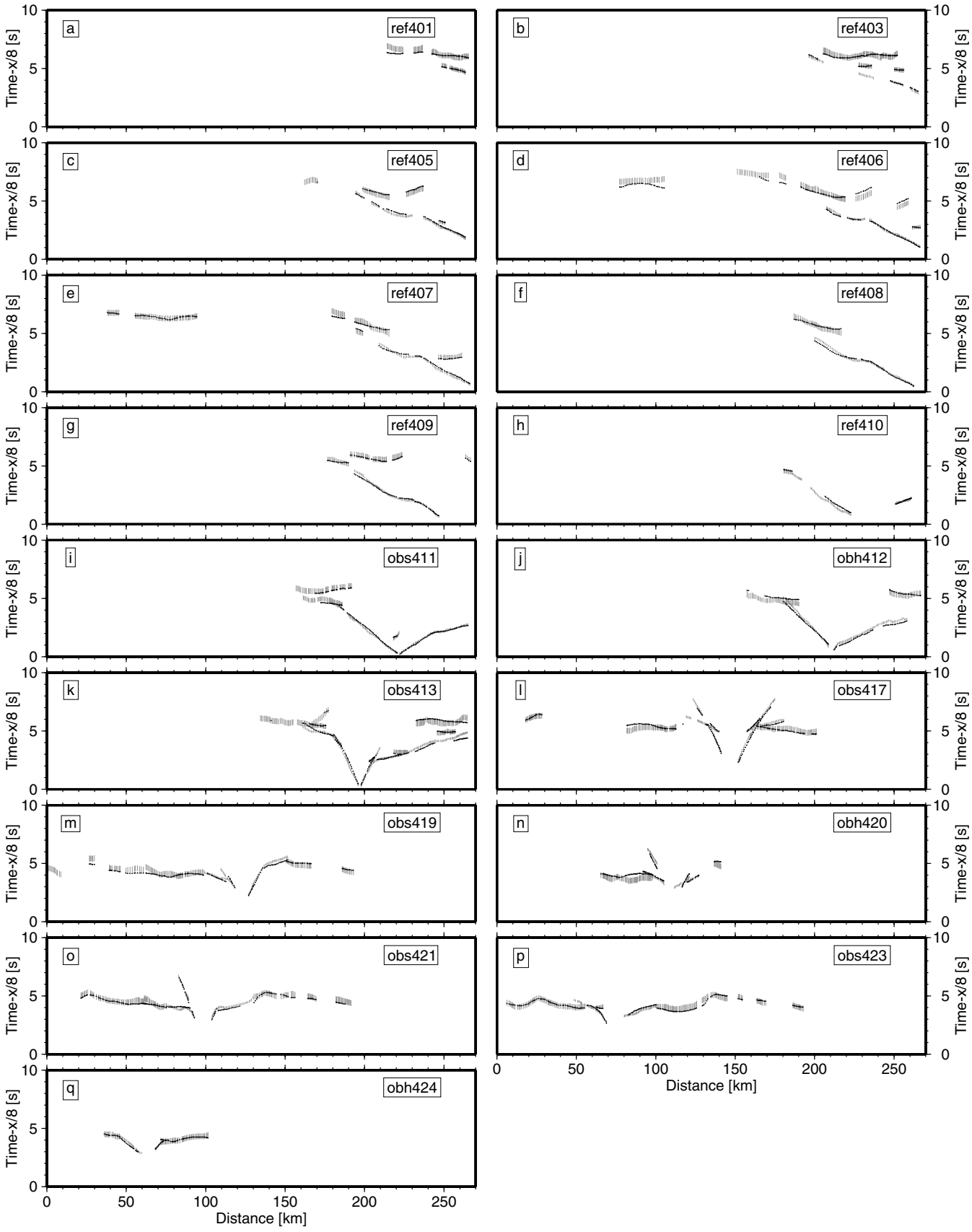

Figure 4. Observed and calculated *P*-wave arrivals for profile AWI-99400: observed and calculated *P*-wave arrivals for profile AWI-99400. (a)–(h): RefTek seismometer systems (ref). (i)–(o): ocean-bottom seismometer/hydrophone systems (obs/obh). Grey errors bars indicate the assigned error to the picked traveltimes. The black lines show the traveltimes calculated using the final velocity model shown in Figs 6 and 7.

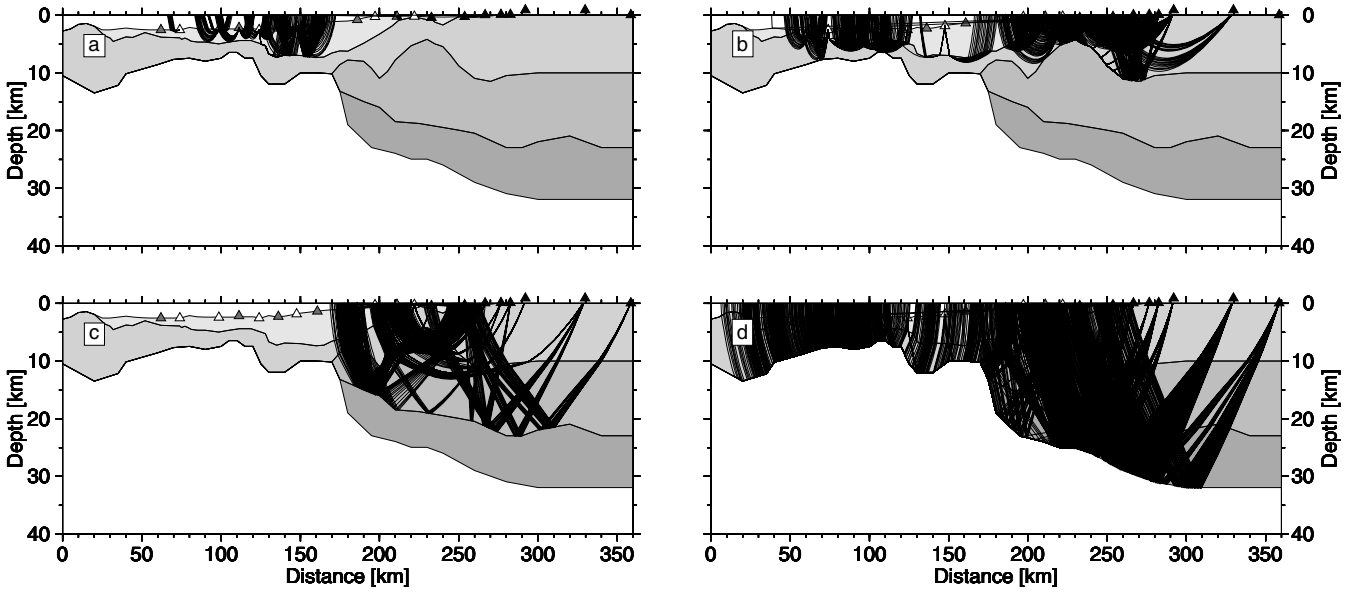

Figure 5. ray tracing for profile AWI-99400: ray tracing for profile AWI-99400 for the five modelled layers (excluding water). (a) Cenozoic sediments and sedimentary rocks. (b) upper crust. (c) middle crust. (d) lower crust and mantle. Vertical exaggeration × 3.

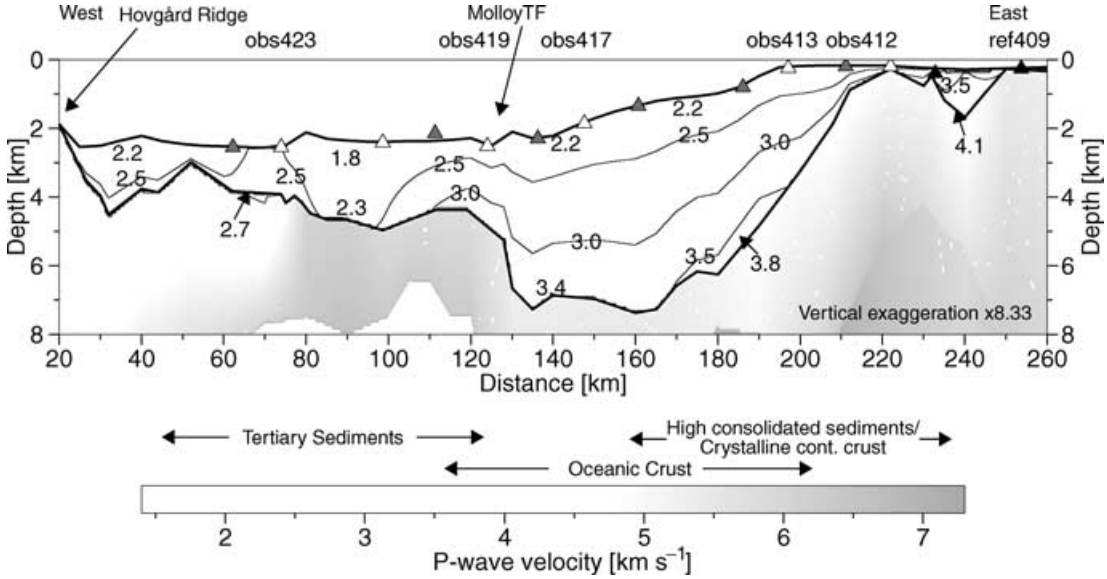

Figure 6. (Final *P*-wave velocity model profile AWI-99400—sedimentary section.) Final *P*-wave velocity model for the sedimentary cover along profile AWI-99400. The contour lines (2.5, 3.0 and 3.5 km s^{-1}) and values shown in the figure indicate seismic *P*-wave velocity. Triangles as for Fig. 1. Vertical exaggeration: × 8.33.

as a result of several wide-angle reflections providing good ray coverage. Upper-mantle resolution values are approximately 0.8 below the eastern continental profile section, but can only be determined west of 250 km.

Resolutions for the oceanic crustal section and the upper mantle below are also variable (Fig. 9b). Values of 0.3 to 0.7 are calculated for the crustal parts, but are slightly lower in the upper mantle.

Empiric analysis of layer depth uncertainty

The uncertainty of the depth levels of the modelled layer boundaries, that are mostly constrained by wide-angle reflections were tested by shifting the depth values of the individual layer boundaries up and down until the calculated traveltime exceeded the assigned error of the pick. The assigned traveltime errors vary between ±100 and 200 ms, depending on the quality of the phase registration. Therefore this empirical test is strongly dependent on the assigned errors to the picks. Because the period is approximately 100 ms our assigned uncertainty include at least one, but at most two, possible misinterpretations of the correct phase traveltime.

We found that depth determination in the top 10 km of the crust has a maximum error of ±0.7 km, if the assigned traveltime errors do not exceed ±100 ms. This results in a maximum error of 10 per cent of the absolute-depth level. Downwards the depth uncertainty increases

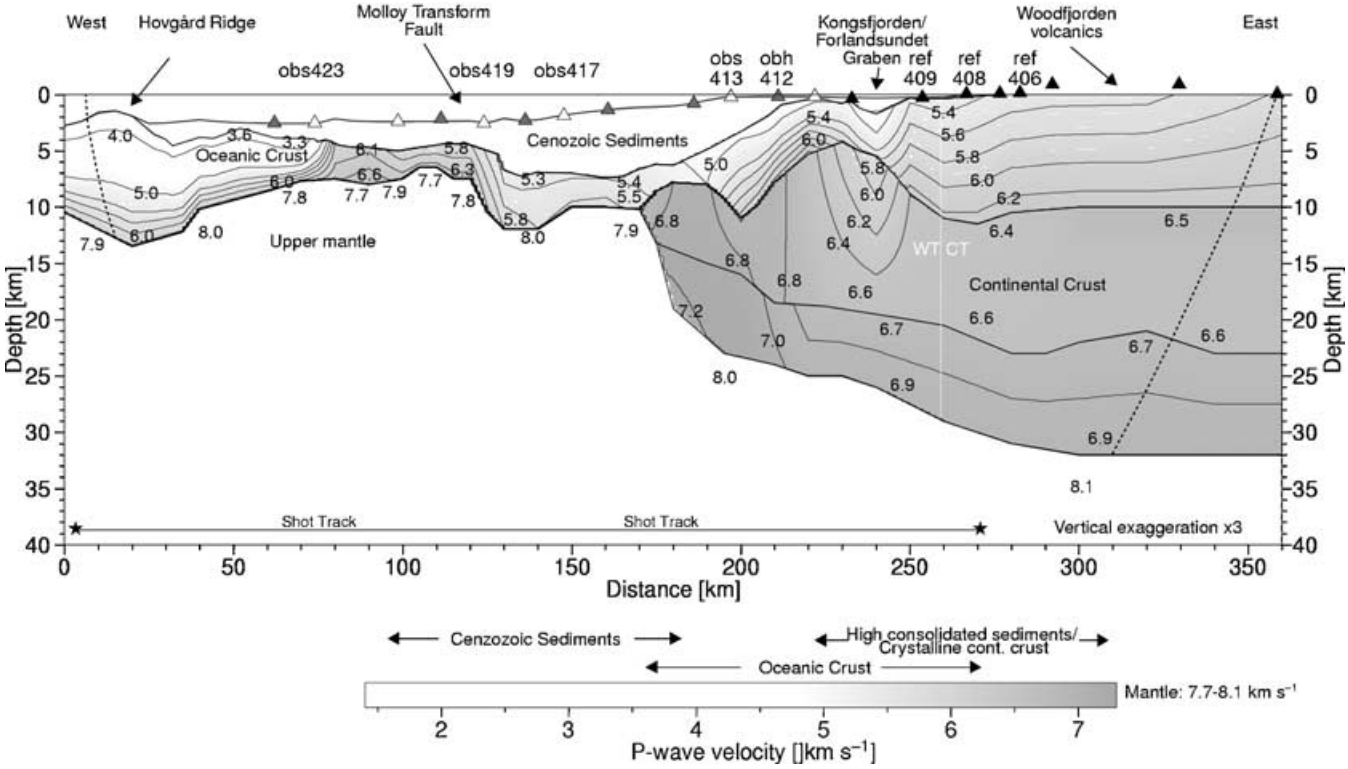

Figure 7. (Final *P*-wave velocity model profile AWI-99400—entire crust.) Final *P*-wave velocity model for profile AWI-99400. The grey shade shows the seismic velocity field, as do the contour lines (4.0 and 5.0 km s^{-1}; 5.4–6.8 km s^{-1}, 0.2 km s^{-1}interval). Triangles as for Fig. 1. The southern and northern maximum extents of penetrating rays are marked by dashed lines. The white dashed line marks the approximately boundary between the western and eastern terrane of Svalbard's Caledonian orogeny. Vertical exaggeration is × 3.

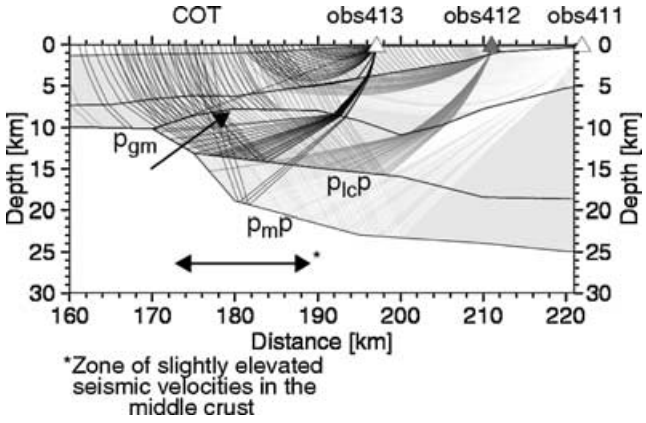

Figure 8. (Ray tracing of seismic stations at the continent–ocean transition.) The diagram shows the ray tracing of stations obs413 (black rays), obh412 and obs411 (grey rays) that constrain the structure of (slightly stretched) continental crust at the continent–ocean transition. Very thin oceanic crust up to 175 km is evidenced by early P_n phases recorded on station obs417 (see Fig. 3f). The continuation of the lower crustal reflector and the continental Moho up to 175 to 180 km is defined by $P_{lc}P$ and P_mP phases. These are recorded by the two eastern stations (grey rays). Moreover, a high-velocity P_{gm} phase recorded by station obs413 (modelled as head wave, see arrow) constrains the elevated seismic velocities at shallow levels at the COT (∼10 km depth).

slightly to values of ±0.9 km independent of the assigned errors of ±150 to ±250 ms. Consequently, the mismatch is approximately 6 per cent of the absolute-depth levels of 10 to 32 km of the middle and lower crustal levels.

Table 2. Modelling results. Continental crustal section included ∼170 to 360 km, (11 stations); oceanic crustal section includes ∼0 to 170 km and offshore Cenozoic sediments, (six to eight stations). The assigned errors are minimum–maximum and average values. RMS misfit and χ^2 after Zelt & Smith (1992).

Section	Phase	Picks used	Assigned errors [s]	RMS misfit [s]	χ^2
Continental section	P_{pb}	15	0.25–0.25, 0.25	0.47	3.85
	P_{uc}	449	0.10–0.10, 0.10	0.15	1.78
	P_{mc}	289	0.10–0.25, 0.15	0.21	1.68
	P_n	197	0.25–0.25, 0.25	0.22	0.78
	$P_{mc}P$	37	0.15–0.15, 0.15	0.14	0.91
	$P_{lc}P$	180	0.20–0.20, 0.20	0.19	0.93
	P_mP	437	0.25–0.25, 0.25	0.20	0.66
Oceanic section	P_{cb}	206	0.10–0.20, 0.14	0.27	2.59
	$P_{cb}P$	37	0.10–0.10, 0.10	0.10	1.08
	P_{go}	194	0.10–0.15, 0.11	0.15	1.65
	P_n	595	0.25–0.25, 0.25	0.25	1.07

Empiric analysis of layer velocity uncertainty

Empirical analysis of the seismic velocities is unequally more difficult to perform. If the modelled traveltime branches do fit the picked (= observed) traveltimes within their given uncertainty, and reverse shots do constrain dip of subsurface horizons, the seismic velocity distribution is one possible model. Nevertheless, the general experience during ray tracing modelling is that mostly a medium model is created to fit the entire range of seismic traveltime picks all along the profile. Positive and negative deviations of the measured seismic velocities (i.e. the slope of a traveltime branch) on adjacent seismic

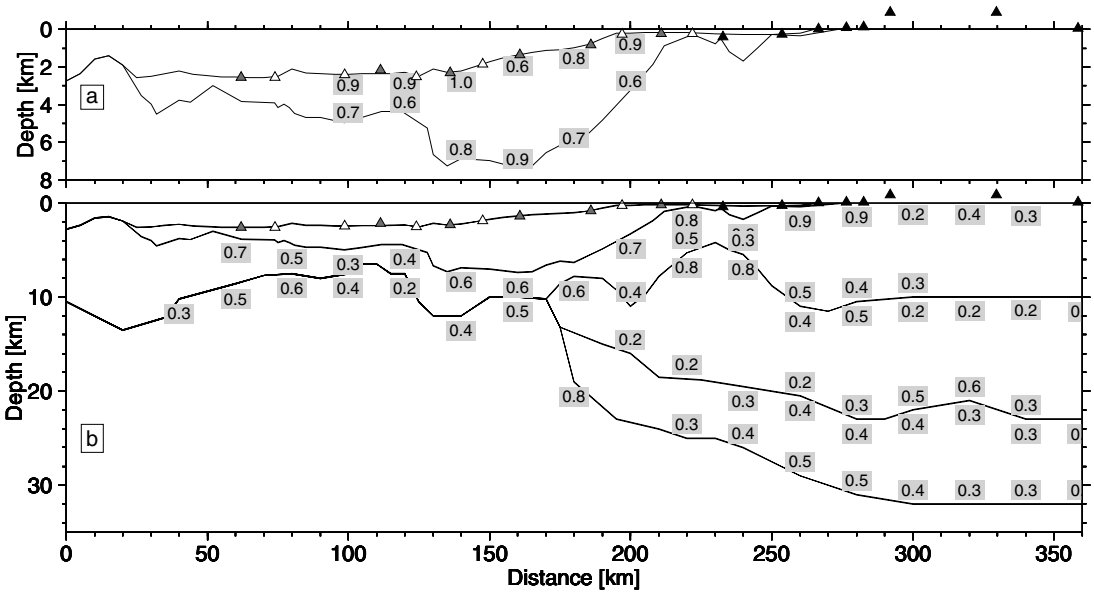

Figure 9. (Resolution of the final *P*-wave velocity model.) Resolution of the *P*-wave velocity field according to Zelt & Smith (1992) resampled to 20 km intervals. Triangles as for Fig. 1. The upper figure (a) shows values for the sedimentary section, the lower figure (b) for the residual crust.

recordings may arise from a non-linear experimental setup, navigational errors, false location of seismic receivers (ocean-bottom devices), non-resolvability of seismic layers or 3-D subsurface structures. Hence, a single seismic recording might show the true subsurface seismic velocity distribution and cannot be rejected easily.

Therefore, we provide the maximum deviation (or tolerance) of seismic velocities as a parameter of uncertainty: after creation of the final medium velocity model, every single seismic station was modelled, without notice of other stations along the profile. The inversion algorithm of Zelt & Smith (1992) was applied to minimize the RMS misfit. The model horizons of the final model (derived by all seismic stations) were held fixed, because only the deviation in seismic velocity was checked. Afterwards, the minimum and maximum deviations of all single-station models from the final model was calculated. Figure 10 shows the exemplary results for the upper and middle crustal layers along a very sensitive section of the profile, the continent–ocean transition (see also Fig. 8 for ray coverage). The gross tolerances are ranging between 0.05 to 0.1 km s^{-1} for the upper crust and 0.1 to 0.2 km s^{-1} for the middle crust.

Interestingly the positive deviations (up to 0.4 km s^{-1}) in the middle crust where slightly higher than the negative. Rather than the upper limit, our presented final velocity model shows in the middle crust most likely the lower limit of allowable seismic velocities (7.2 km s^{-1}). This fact is hardly negligible, because high seismic velocities within the continent–ocean transition are commonly interpreted as MgO-rich volcanic intrusions. We therefore conclude that the elevated seismic velocities at the continent–ocean transition have to be considered for subsequent geological interpretation.

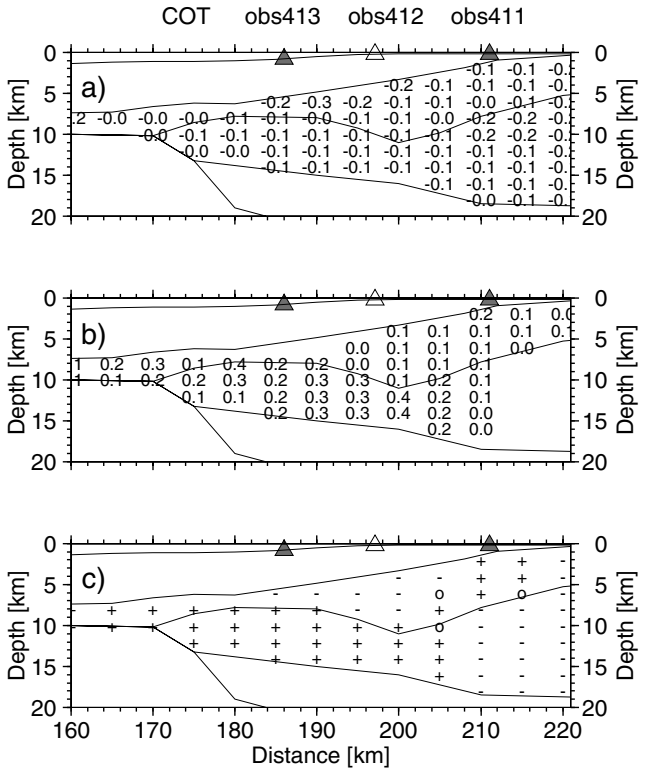

Figure 10. (Minimum–maximum deviations of the seismic velocities at the continent–ocean transition.) Minimum and maximum deviations (tolerances) of seismic velocities within the upper and middle crust along continent–ocean transition. Deviations are shown by a grid pattern of 5 × 2 km. (a) Minimum deviation. (b) maximum deviation. (c) sum of (a) and (b), a parameter of underestimation (+) or overestimation of seismic velocities.

Gravity data acquisition and characteristics

Gravity data were acquired along the shot track by RV Polarstern with the shipboard gravity meter. Processing comprises integration to the International Gravity Standardization Net 1971 (IGSN71) using harbour links at Tromsø(Norway) and Bremerhaven (Germany). Further, an Eotvös correction was applied to obtain the free-air gravity anomaly. Data for the onshore section east of Kongsfjorden was extracted from the free-air anomaly grid of the Svalbard/Greenland region of Boebel (2000) and adjusted to the processed ships gravity.

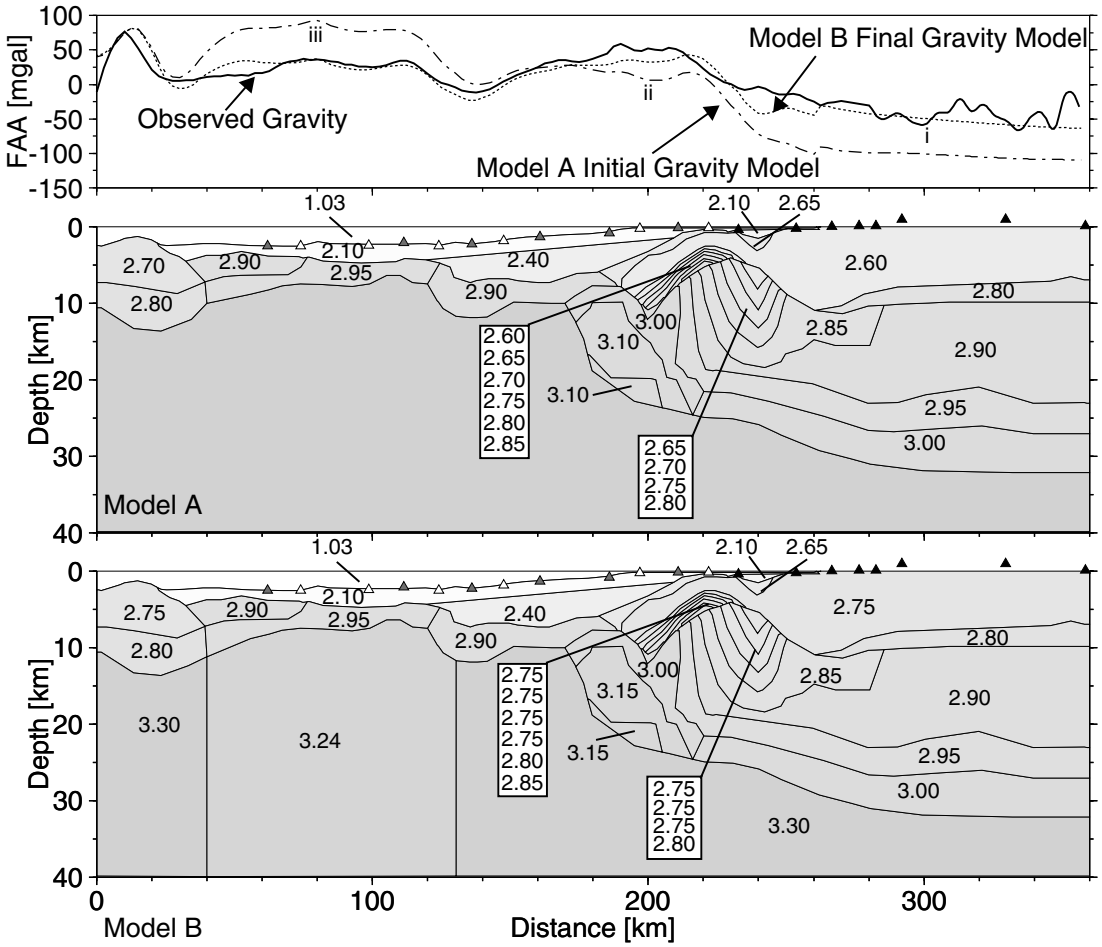

Figure 11. Initial and final density models and free-air anomaly for profile AWI-99400: initial (model A) and final (model B) density models for profile AWI-99400. The observed free-air anomaly is marked by a thick solid line in the upper graph. The derived free-air anomaly from model A is marked by a dashed-dotted line, from model B by a dotted line. For calculation of densities and modelling parameters see text. Triangles as for Fig. 1.

The anomaly variation along the entire profile is approximately 145 mGal (Fig. 11: −65 mGal at 334 km, 80 mGal at 10 km). Gravity increases towards the west along the onshore section of the profile from −50 to 0 mGal, with some short-wavelength anomalies from 300 to 360 km. At approximately 200 km a gravity maximum of 60 mGal is observed forming a 40 km wide anomaly. Gravity decreases continuously towards Molloy Transform Fault at 140 km. The oceanic crustal section to the west is characterized by a plateau with gentle undulations. The Hovgård Ridge at the western edge of the profile terminates the gravity record by a strong, 75 mGal positive anomaly peak.

Gravity modelling

The *P*-wave velocity model presented above was gridded and transformed into an initial density model using the non-linear velocity–density regression of Christensen & Mooney (1995). This relation includes mantle rocks, such as dunite and pyroxenite, and is therefore suitable for crust–mantle studies. Subsequently, blocks were digitized within an interval of 0.05 g cm^{-3}. Rock densities for the sedimentary cover were set to 2.10 and 2.40 g cm^{-3}; the mantle density is uniform 3.3 g cm^{-3}. The potential field data interpretation software LCT was used to model free-air gravity.

Model A in Fig. 11 shows the calculated density model as described above. It is obvious that the model does not fit the observed gravity field:

(i) There is a −50 mGal misfit along the mostly unstretched continental section of the profile.
(ii) There is a +50 mGal misfit at 200 km.
(iii) There is a 60 mGal misfit over the region between the Hovgård Ridge and Molloy Transform Fault.

We applied the following modifications to the density model to eliminate these misfits (Fig. 11; model B):

(i) Raising density of the upper part of the eastern continental section to 2.75 g cm^{-3}. This is consistent with density measurements on field rock samples published by Kurinin (1970) and Howells *et al.* (1977). Kurinin (1970) report on mean group densities of 2.68 to 2.72 g cm^{-3} for Devonian and lower metamorphic rocks. Howells *et al.* (1977) defined formation densities of 2.72 to 2.76 g cm^{-3} for pre-Devonian to Devonian rocks of northern Svalbard.
(ii) Further west, densities of the zone of slightly increased seismic velocities (Fig. 11; 200 km) are raised to 3.15 g cm^{-3}.
(iii) Between Hovgård Ridge and Molloy Transform Fault the mantle density of 3.30 g cm^{-3} was decreased to 3.24 g cm^{-3}, to produce a downward shift of calculated gravity values by approximately 60 mGal. Lower mantle densities of 3.26 g cm^{-3} are also suggested

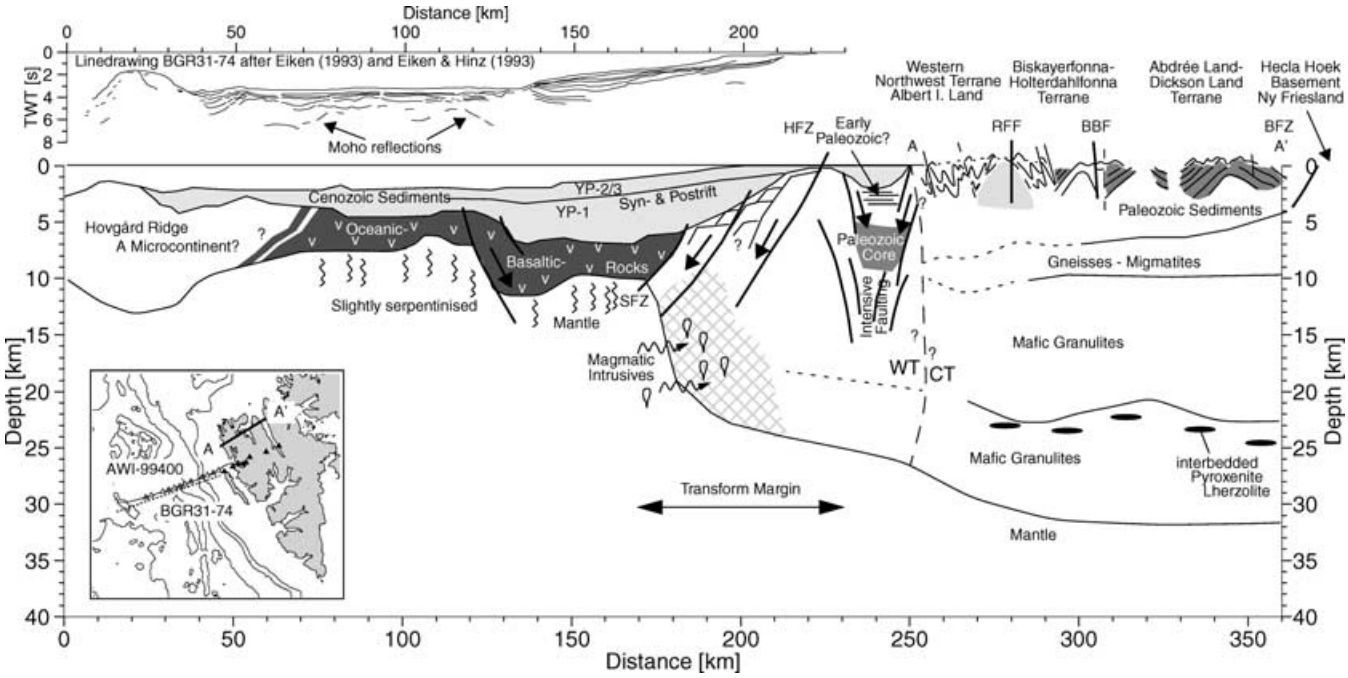

Figure 12. Geological interpretation of profile AWI-99400: geological interpretation of the velocity model along profile AWI-99400. For the oceanic crustal section a line drawing of multichannel line BGR31-74 (Eiken 1993; Eiken & Hinz 1993) is shown. See insert map for location (dotted line). Note that the steep Moho topography at the Molloy Transform Fault was observed on the multichannel transect. The eastern continental section also shows a geological cross-section for northwestern Svalbard (A-A'; after Hjelle & Lauritzen 1982). The geological profile is marked on the insert map by a thick black line. Generally, continental crust is coloured white, oceanic dark grey. The mid-grey colour indicates Palaeozoic sedimentary rocks. The crosshatch pattern marks the zone along the sheared margin that is intruded, as characterized by higher seismic velocities (up to 7.2 km s^{-1}). The vertical dashed line at 250 km marks approximately the boundary between the western and central terrane of Svalbard. HFZ: Hornsund Lineament. RFF: Raudfjorden Fault. BBF: Breibogen Fault. BFZ: Billefjorden Fault. SFZ: Spitsbergen Fracture Zone.

for the Northern Atlantic Senja margin (Breivik *et al.* 1999) by modelling the thermal structure of the lithosphere. Below Hovgård Ridge the mantle density of 3.30 g cm^{-3} remains unchanged because the gravity calculation using model A fits the observed field well.

The final density model

The final density model B (Fig. 11) gives further constraint to the modelled velocity structure. The crustal density variations of model B compared to the initial model A, imply velocities that are within the given uncertainties of the final velocity model and the non-linear regression of Christensen & Mooney (1995). The negative shift in mantle density of approximately 0.1 g cm^{-3} below the oceanic crustal section is consistent with the relatively low observed seismic velocities of 7.7–7.8 km s^{-1} in the upper mantle. The high densities of 3.15 g cm^{-3} within the middle crust at 200 km may point to an underestimation of the seismic velocity of 7.2 km s^{-1} at this location. The recalculation of the seismic velocity from the modelled density derives values of 7.4 km s^{-1}. This fits to the discussion of possible tolerances of seismic velocities where similarly an underestimation is observed.

INTERPRETATION AND DISCUSSION

For further discussion and interpretation of the velocity and density structure the profile AWI-99400 is split into four individual sections:

(i) The Cenozoic sedimentary cover from 20 to 245 km, which overlays continental, transitional and oceanic crust.

(ii) The eastern continental section east of 200 km, which covers parts of the proposed western and central terrane of the Svalbard archipelago. In the upper levels it is characterized by a 8 km thick Palaeozoic sedimentary basin, known from geological record (Fig. 1).

(iii) The transition to the oceanic domain to the west, that features a steep Moho uplift of 15 km, a zone of slightly elevated seismic velocities and a pronounced density anomaly.

(iv) The oceanic section of the profile west of 170 km, which is subdivided into two sub-regions by the Molloy transform fault at 120 km.

The interpretation of the different sections is summarized in Fig. 12.

The Cenozoic sedimentary cover east of Molloy transform Fault

Seismic reflection data published by Eiken & Hinz (1993) and Eiken (1993) shows three sedimentary sequences (YP-1 to YP-3; Fig. 12) for northwestern Svalbard and the adjacent Yermak Plateau. Geissler (2001) attributed sonobuoy-derived seismic velocities to the individual sequences. The seismic velocities are defined as follows: 3.2 to 4.2 km s^{-1} for YP-1 (lower), 1.9 to 2.4 km s^{-1} for YP-2 (middle) and 1.7 to 1.8 km s^{-1} for YP-3 (upper). A comparable velocity structure is also found for the lower sequences in the northern Barents sea (Fig. 1b; Myhre & Eldholm 1988, ESP1-5; 3.2 to 4.3 km s^{-1}, 1.9 to 3.2 km s^{-1}), so that a regional trend can be deduced. The observed seismic velocities along profile AWI-99400 indicate the presence of sequences YP-1 and YP-2. Henceforward, we will take 2.4 km

s^{-1} to mark the approximate boundary between YP-1 and YP-2. The applied low-frequency air-gun source limits the resolution of the shallowest sequence, YP-3.

Eiken (1993) suggests a latest Oligocene (36 Ma) to the Late Miocene (7 Ma) age for YP-1. The youngest strata of YP-2 are supposed to be Early Quarternary. Our data thus show more than 4 km of YP-1 strata west of the Molloy Transform Fault (Fig. 1a). According to the estimated age, this sequence comprises syn- and post-rift sediments and sedimentary rocks. The work of Steel *et al.* (1985) indicates that Early to Middle Palaeocene clastics were deposited on either side of the uplifting west Spitsbergen fold belt during transtensional movements. Therefore, the lower parts of YP-1 may comprise Palaeocene strata.

The eastern continental section

This profile section covers the parts of the western and the central terrane of Svalbard (station ref409 (Figs 1a and 2) is approximately located at the bounding Kongsfjorden–Hansbreen Fault Zone).

Central terrane (250 to 360 km)

Geological cross-sections of the central terrane cut through several exposed basement provinces (or subterranes), i.e. the western NW terrane of Albert I Land to the west of the Raudfjorden Fault Zone, the Biskayerfonna–Holterdahlfonna terrane west of the Breibogen Fault Zone and the Andrée Land–Dickson Land terrane west of the Billefjorden fault zone (Fig. 1a; Hjelle & Lauritzen 1982). Although the lithology of each terrane is extremely varied, this is not reflected in the observed velocity structure. The modelled seismic velocity is distributed uniformly in the upper crust, with only slight changes suggesting the presence of the metamorphic rocks of Albert I Land and the Hecla Hoek province east of Billefjorden Fault Zone.

We suggest the lower sequences of the Devonian basin (Fig. 1a) are located at depths of 4 to 7 km following the 6.1 km s^{-1} isocontour, the maximum seismic velocity observed for Palaeozoic strata of the Svalbard–Greenland depositional realm (e.g. Jackson 1990; Hajnal *et al.* 1990; Schlindwein & Jokat 1999).

In petrological models of the deeper structure of Svalbard's central terrane (more precisely the basement province east of the Breibogen Fault Zone; Fig. 1a; Amundsen *et al.* 1987), the crust is built up of three rock units, regionally overlain by Palaeozoic sedimentary rocks. The proposed rock types are:

(i) Gneisses.
(ii) Granulites.
(iii) Granulites with small amounts of interbedded pyroxenite/lherzolite (observed on mantle xenolithes).

The latter unit is most likely not associated with large igneous intrusives related to mantle plume activity, because new seismic refraction data from the Yermak Plateau do not support a Yermak hotspot (Ritzmann & Jokat 2003). The rock units (i), (ii) and (iii) were related to velocities of 6.1 to 6.3 km s^{-1}, 6.4 to 6.6 km s^{-1} and 6.7 to 6.8 km s^{-1}, respectively (Chan & Mitchell 1982). Our results for the central terrane reinforce these models. Granulitic rocks are therefore supposed at depths between 10 and 22 km. Similar seismic velocities (6.1 km s^{-1}) for the upper crystalline layer are reported for the Isfjorden region 100 km further south (Sellevoll *et al.* 1991). The origin of lower crustal reflectivity is under debate (Mooney & Meissner 1992). The observations of Amundsen *et al.* (1987) on xenolithes of mafic intrusions in the lower crust seem to be a likely cause. In this case, the reflective horizon at 22 km depth indicates that lower crustal interbedded material possibly raise up to a certain depth level, probably defined by uniform P–T conditions or the brittle/ductile transition. Moreover, lower crustal reflectivity may be caused by the process of extension (Mooney & Meissner 1992). Ductile flow in the lower crust aligns minerals and stretches lower crustal bodies. Throughout the Cenozoic, extension and later rifting dominated the Svalbard realm. Further, Ritzmann & Jokat (2003) report an Oligocene simple shear extension on the southern Yermak Plateau. On the basis of our data alone, it is not possible to reveal the origin of the lower crustal reflection, although we favour low amount of intrusions based on mantle xenolith samples.

A transitional crust–mantle boundary below Svalbard as suggested by Sellevoll *et al.* (1991) and Czuba *et al.* (1999) can not be confirmed for the northern region (velocities between 7.35 and 7.8 km s^{-1}). Instead our seismic model shows a first-order crust–mantle transition (Figs 7 and 12).

Western terrane (210 to 250 km)

The western terrane (Fig. 1a) is characterized by an abrupt decrease of seismic velocity and rock density to depths of 20 km directly below the Forlandsundet graben (Fig. 7) within the Tertiary western Spitsbergen orogenic belt (Fig. 1b). The Caledonian geological suture between the central and western terranes at 255 km (Harland & Wright 1979) is not evident in our model. The Tertiary break-up of Svalbard and northern Greenland is supposed to have mainly involved strike-slip movements along the Hornsund Lineament to the east of this low-velocity structure since Oligocene times (Eldholm *et al.* 1987).

The development of the Forlandsundet graben within a mainly compressional fold and thrust belt is speculative. The general age of the sedimentary infill is Late Eocene to Oligocene. An extensional or transtensional event during (prior?) to the continental break-up from Greenland is supposed to have caused subsidence (Dallmann *et al.* 1993).

Nevertheless, a strike-slip/pull-apart character for the Forlandsundet graben is mentioned in earlier work (e.g. Lepvrier & Geyssant 1985; Steel *et al.* 1985; Harland 1997c). An old assumption for the fold belt development was proposed by Lowell 1972. Within a convergent strike-slip zone crustal sheets were thrusted up to result in a typical flower structure. Later, the Forlandsundet graben developed possibly as a collapse graben along the axis of the main fold belt (Steel *et al.* 1985).

It is not possible to examine the tectonic regime in detail. Though, the observed low seismic velocity zone beneath the Forlandsundet graben may interpreted as a deep axial fault zone. Rock formations within this zone might be fractured during the entire Tertiary tectonic processes related to the Svalbard–Greenland break-up. This zone lies in close proximity to the Caledonian suture (i.e. Kongsfjorden–Hansbreen Fault Zone) which leads to the assumption that possibly Tertiary movements reactivated an older shear zone.

In addition to a tectonic cause, parts of the low seismic velocities below 6.0 km s^{-1} might represent Palaeozoic sedimentary rocks as in the upper crust of the central terrane. Accordingly, any narrow sedimentary trough would be downfaulted approximately 4 km, i.e. the throw of the Forlandsundet graben (Eiken & Austegard 1987). Deeper seated Palaeozoic rocks were also found below the Oligocene Danskøya Basin (Fig. 1a; Eiken 1993) approximately 120 km further north (Ritzmann & Jokat 2003). In a similar way, at the Forlandsundet graben a 5 km Tertiary sequence may cover

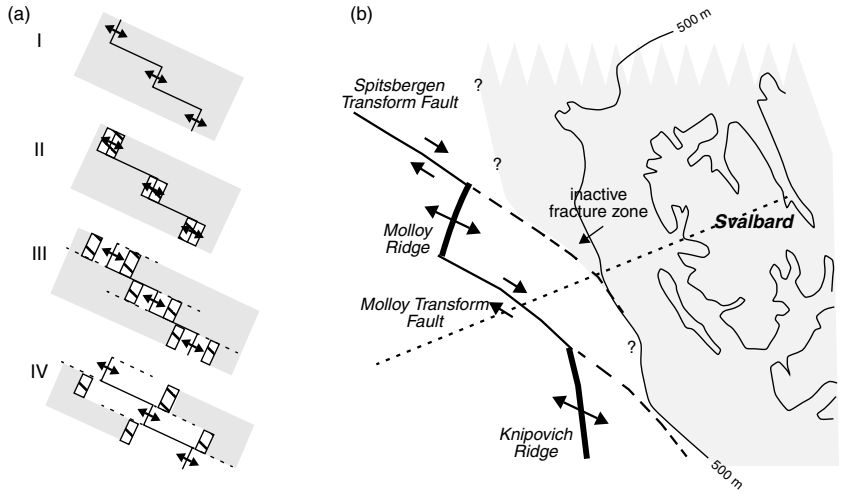

Figure 13. Sheared margin development—proposed southeastern extent of Spitsbergen Transform Fault. (a) Schematic evolution of a transform (sheared) continental margin. Grey: Continental crust. Hatched: Stretched continental crust. White: Oceanic crust. Phase I: Development of continental transform faults. Phase II: Crustal stretching between continental transforms. Phase III: Development of an active transforms separating oceanic from continental crust. Phase IV: The spreading ridges had passed the continental section and the active transform becomes an inactive fracture zone. (b) schematic map of the proposed southeastern extension of the Spitsbergen Transform Fault to the inactive fracture zone (dashed line, east of Molloy Ridge). Grey colour marks the location of observed (stretched) continental crust (this study and Ritzmann & Jokat 2003). Thick lines are spreading ridges, and thin continuous lines are the respective transform faults between. The dotted line marks the approximate position of profile AWI-99400. Bathymetry: sketched from IBCAO (Jakobsson *et al.* 2000).

deeper Palaeozoic rocks, within a probable transtensional graben setting. The preservation of Devonian sedimentary rocks within the Tertiary fold belt is also observed onshore in the region of the Hornsund (Fig. 1a; e.g. Steel *et al.* 1985).

In summary, we interpret the upper/middle crust below Forlandsundet graben to consist of both downfaulted Palaeozoic sedimentary strata and extensively fractured rocks.

Further west, off Prins Karls Forland, the profile crosses the Hornsund Lineament (Eiken 1993). Like the Caledonian suture (at 255 km) a deeper structure of the Hornsund Lineament is not clearly visible. The fault may follow the isovelocity contour of the upper crystalline layer, in a westward dipping (listric?) manner. Published seismic reflection data (Eiken & Austegard 1987; Eiken 1993) show that the lineament consists of two separate blocks at Sjubrebanken, north of Prins Karls Forland. Our deep seismic data off Kongsfjorden do not define the internal structure of the lineament. The absence of stepwise deepening of the upper basement below the shelf sedimentary rocks may point to an unfaulted structure here. The striking manifestation of the Forlandsundet graben compared to the absence of striking features for the Hornsund Lineament suggests that the two structures have separate, and rather different tectonic histories.

The continent–ocean transition

The continent–ocean transition along profile AWI-99400 is characterized by a rapid change in Moho depth on the eastern continental section which gives way to thin oceanic crust at 170 km. This transition is characterized by the highest seismic velocities found for continental crust along the profile (7.2 km s^{-1}). The maximum steepness of the Moho along profile AWI-99400 is directly east of the transition, where the Moho dips at angles of 45° from 10 to 20 km depth. The rapid decrease of Moho depth at the continent–ocean transition may be characteristic of sheared or transform continental margins. At such margins, complex rifting occurs along a continental transform fault (Fig. 13a; phase I and II), followed by the development of an active transform boundary separating oceanic from continental crust (Fig. 13a; phase III; Lorenzo 1997). Later the ridge passes the continental section and the transform becomes inactive apart from differential subsidence (Fig. 13a; phase IV).

Fig. 13(b) shows the proposed scenario for the observed continental margin along profile AWI-99400 and the adjacent plate boundary in the Fram strait. The continent–ocean transform off northern Prins Karls Forland is located along the southern extension of Spitsbergen Transform Fault, today represented by an inactive fracture zone. The southeasterly trend of this fracture zone towards Prins Karls Forland dictates, therefore, most likely the occurrence of (stretched) continental crust (shaded in grey; Fig. 13b). Additional support for this hypothesis is given by two facts:

(i) At transform continental margins spreading anomalies in the adjacent oceanic crust appear perpendicular to the margin. Recently acquired helicopter based magnetic data between the northeast Greenland shelf and the Molloy Ridge reveal well defined magnetic anomalies parallel to the ridge axis (Jokat *et al.* 2003). Hence, a similar ridge-parallel anomaly pattern (=perpendicular to the inactive fracture zone) is expected between Molloy Ridge and the Svalbard margin.

(ii) A seismic refraction profile along the northern coast of Svalbard to the Molloy deep (Fig. 1a) shows clearly the occurrence of (stretched) continental crust east of 6°E (Ritzmann 2003). This yields further reliability to the proposed track of the inactive fault that bounds (stretched) continental crust from oceanic crust.

The crustal structure of other sheared margins that are constrained by seismic experiments is well known from the Côte d'Ivoire, Ghana margin (Edwards *et al.* 1997), the eastern Canada margins (Reid 1988; Todd *et al.* 1988; Reid & Jackson 1997) off Queen Charlotte Island (Horn *et al.* 1984), the Exmouth Plateau (Lorenzo *et al.* 1991) and the nearby Senja–Barents sea margin (Faleide *et al.* 1991).

The Côte d'Ivoire, Ghana margin shows a similar extreme topography of the Moho to that observed along profile AWI-99400. The other margins are characterized by a broader, 30–60 km wide transition zone. Comparing the velocity structure of these margins, high

seismic velocities are common at the continent–ocean transition. In the case of the Côte d'Ivoire, Ghana margin, oceanic and continental crust are separated by a high seismic velocity unit (5.8 to 7.3 km s^{-1}). The cause of these velocities is ambiguous: the interfacing body is either interpreted as emplaced lower crustal/mantle rocks or heavily intruded basic igneous rocks (Edwards *et al.* 1997). Intrusions might occur in the presence of a slight transtensional stress component making the ancient transform slightly leaky. The nearby Senja margin (Eldholm *et al.* 1987) exhibits such leaky behaviour because volcanic activity and similar high seismic velocities are found within the crust (7.1 km s^{-1}). Horn *et al.* (1984) modelled a 20 km wide body (5.5 to 7.4 km s^{-1}) at the transition of the Queen Charlotte margin as sheared basalts and gabbros. This body extends down to depths of 17 km, showing a deepening lower edge towards the continent, and is similar to that found along our profile. It is uncertain whether the Queen Charlotte margin body has a continental or oceanic character (Horn *et al.* 1984).

In summary, we deduce that the sheared margin off Prins Karls Forland differs in detail from those reported above, because an altered high-velocity section of continental crust is observed (Fig. 7; 170–300 km). As a result of the transtensional stress field prior to the actual opening of the Fram strait, the continental crust on the eastern side of the transform was affected by (oblique) stretching (200 to 240 km along the profile). Moreover, a significant amount of mantle-derived melts may contaminate the lower and middle crust at the transition, raising the velocity here, however, its origin remains speculative. According to Lorenzo *et al.* (1991), the large temperature contrast over juvenile transform margins might result in convection-induced secondary melting of the upper-mantle (referring to Mutter *et al.* 1988). This may lead to intrusions during the passage of the ridge segment and/or hot oceanic crust. Further, the melt supply might occur by a simple ridge–continental crust interaction during transit of the hot Molloy Ridge along sheared continental crust.

The western oceanic section

Oceust (45 to 170 km)

The profile covers two ancient oceanic crustal sections, on each side of the plate boundary (i.e. Molloy Transform Fault; Fig. 1a). The section to the east was formed at the Molloy Ridge spreading segment, while that to the west is formed at the Knipovich Ridge. An age prediction of the surveyed crustal sections is difficult because magnetic data of sufficient quality is missing. Magnetic data of Verhoef *et al.* (1996) reveals no regular spreading anomalies for the northern Knipovich Ridge. New acquired magnetic data of the northwestern segment of Molloy Ridge reveal spreading anomalies (Jokat *et al.* 2003), however, a recent dating of single anomalies is not available. Using the synthetic flow-lines of Eldholm *et al.* (1990) chron 5 (∼9.5 Ma) should occur ∼70 km off the Knipovich Ridge at 77°N (based on Talwani & Eldholm 1977). Our profile AWI-99400 obliquely intersects the Molloy Transform Fault (130 km length; Crane *et al.* 2001) roughly half way between the two ridge–transform intersections. The surveyed crustal sections are 70 to 100 km off the axes of the spreading centres. We therefore conclude that the age ranges roughly between 10 and 15 Ma (Middle Miocene), keeping in mind that Crane *et al.* (1991) mentioned the possibility of extremely asymmetric spreading rates at the Knipovich Ridge.

The absence of seismic velocities higher than 6.6 km $s^{-1}$is very prominent and reflects the absence of oceanic layer 3 along the profile. Further, this excludes a serpentinization front to the Moho (Minshull *et al.* 1998). Velocities vary between 5.3 and 6.6 km s^{-1}on either side of the Molloy Transform Fault and total thicknesses of the igneous portion range between 2 and 4.5 km. This is thin compared to the global mean of approximately 7.1 km, based on seismic experiments (White *et al.* 1992).

After Reid & Jackson (1981) crustal thicknesses of mid-ocean ridges decrease sharply for spreading rates below 20 mm a^{-1}. Recent work of White *et al.* (2001) concludes that conductive heat loss is the most important factor inhibiting melt production. According to the observations of Bown & White (1994) crustal thinning is dedicated to the thinning of oceanic layer 3. Because the Knipovich and Molloy Ridges are characterized by slow spreading rates of ∼8 mm a^{-1}(Eldholm *et al.* 1990), the correlation between spreading rate and layer 3 thickness (or absence) fits with our study. The observed crustal thicknesses are in good agreement with those derived by rare earth element inversion (for the Knipovich Ridge) of 2.77 to 4.9 km of White *et al.* (2001). Further, our derived crustal structure is comparable to that of Klingelhöfer *et al.* (2000) parallel to the Mohns Ridge at 72^{-1}N (Fig. 1b). Thicknesses vary around 4 km due to a great variability of layer 3 thickness. It should be noted that the upper basement velocities of layer 2 at the Mohns Ridge are lower than observed along profile AWI-99400 (2.5 to 3.0 km s^{-1}).

The differing seismic velocities for the oceanic layer 2 on either sides of the Molloy Transform Fault remains problematic. One explanation could be that this is simply the result of different ages of the crust. The seismic structure of the oceanic crust may also be a function of tectonics or thermal diffusion effects related to the proximity of the Molloy Transform Fault. The possibility of a different petrology may be a further point of discussion, which will not be debated here.

Molloy Transform Fault (130 km)

The Molloy Transform Fault is characterized by an unusual steep asymmetric topography of the crust–mantle boundary and by an increase of seismic velocity from east to west. Oceanic layer 3 is absent. According to studies of transform faults in the North Atlantic (Detrick *et al.* (1993) note that the authors commonly use the term fracture zones for transform faults and fracture zones) the lack of layer 3 velocities (or higher) within the crust is typical for transform faults with a large offsets greater than 100 km (offset Knipovich to Molloy Ridge is ∼150 km).

A common feature of transform faults in the North Atlantic (e.g. Charlie-Gibbs, Vema; Detrick *et al.* 1993) is the broad symmetrical upwarping of the Moho below the valley and accompanying transverse ridges on both sides. In contrast, the Molloy Transform Fault exhibits a pronounced asymmetric structure. A comparison with seismic reflection data of Eiken & Hinz (1993) and Eiken (1993) shows that the steep topography of the subsedimentary crust was already known (Fig. 12; line drawing). However, arrivals were interpreted as intrabasement reflections assuming a deeper crust–mantle boundary. This study shows that crust at the Molloy Transform Fault is thinner than previously expected. Regarding the basement topography across the transform it seems likely that the transform itself acts as a hinge for differential subsidence of the flanking oceanic sections. This may be have been enhanced by the different sedimentary load. On the eastern side accumulated sediments and sedimentary rocks may amplify the subsidence of the oceanic crust, probably as a result of the vicinity of continental Svalbard. Normal faulting of the region between the Molloy Transform Fault and the Hovgård Ridge

is evidenced by Baturin (1990) and Eiken (1993) in compilation of seismic lines off western Svalbard, which was attributed to moderate extension after formation of igneous crust. Crane *et al.* (2001) suggest that fault traces observed north of the Molloy Transform Fault are due to rifting of the Knipovich Ridge that has propagated north beyond the rift–transform intersection in geologically recent times. For the location of Molloy Transform Fault, both interpretations have to be upgraded and basement subsidence has to be considered to play a substantial role in fault development. A sedimentary sequence of more than 4 km thickness is observed at the transform fault, which is supposed to thicken towards north (Vestnesa, Eiken 1993, Fig. 1a). Therefore, we suppose basement subsidence along the entire transform fault.

Further constraint on a northeast dipping normal fault complex might be given by the work of Okay & Crane (1993). They propose a dipping detachment from the Spitsbergen Transform Fault underneath the Yermak Plateau, which was initiated by simple shear tectonic break-up and later asymmetric spreading. Hence, the trend of the normal faulting at Molloy Transform Fault might be a stress relict from the initial break-up.

Upper mantle

Upper-mantle velocities along the oceanic section of the profile are lower than along the continental section of Svalbard (8.0 to 8.1 km s^{-1}; see also Ritzmann & Jokat 2003), which possibly points to a change in petrology. This is further supported by lower densities, at least for the region to the west of Molloy transform fault. The lowering of mantle seismic velocities may result from a slight serpentinization of upper-mantle peridotites. After Minshull *et al.* (1998) thin oceanic crust, slow spreading ridges and fracture zones all favour serpentinization by providing faulted pathways for seawater to penetrate the upper mantle. In fact, the lowest seismic velocities are found below the Molloy Transform Fault. Further, fractures and faults associated with the Hovgård Ridge, the Hovgård Fracture Zone (Myhre *et al.* 1982) and the transform margin might provide additional pathways for water to reach mantle levels. According to Christensen (1966) and Christensen (1978) ∼20 per cent serpentinization is required to reduce seismic velocity to 7.1 and 7.6 km s^{-1}, whereas the latter is the lowest velocity observed. As the velocity distribution is not homogeneous we expect different degrees of serpentinization. Observed seismic velocities for the upper mantle at the Mohns Ridge are similarly low and attributed to serpentinization as reported by Klingelhöfer *et al.* (2000).

CONCLUSIONS

The seismic refraction profile off Kongsfjorden in Svalbard provides a detailed seismic velocity structure of a sheared continental margin. It also gives new information concerning the geology of central Svalbard and the development and evolution of the northwestern continental margin of Eurasia. The sheared margin off Kongsfjorden is, most likely, slightly influenced by magmatic activity. Svalbard's western continental margin seems to be more segmented as expected. Between Prins Karls Forland and the northern coast of Svalbard, the margin is part of the Spitsbergen Fracture Zone. Further to the south, off Van Mijenfjorden, the crustal structure revealed a normal rifted margin segment with a 100 km wide continent–ocean transition zone (Ritzmann *et al.* 2002). The segmentation into sheared and rifted margin along the Barents sea margin is well established (e.g. Breivik *et al.* 1999, 2003). We therefore conclude that a similar segmentation is also given off western Svalbard.

Our main results are:

(i) The seismic velocity structure does not resolve Caledonian crustal blocks. Late Palaeozoic sedimentary rocks are modelled with a thickness of up to 7 km and additional Palaeozoic sedimentary rocks occur below the Forlandsundet graben. These rock units can be associated with those of Svalbard's central terrane and the lithology found by Amundsen *et al.* (1987).

(ii) The crustal structure of the upper 20 km below Forlandsundet graben exhibits low seismic velocities, interpreted as being the result of intensive faulting during the early Palaeocene movements between Svalbard and Greenland. Because this structure is located adjacent to the proposed (sinistral) Caledonian suture between the western and central terrane, (dextral) Tertiary movements may have reactivated the Palaeozoic shear zone.

(iii) The continent–ocean transition can be classified as a sheared margin, with the Spitsbergen Transform Fault/Spitsbergen Fracture Zone as the trace of the fault. A steep increase (45°) in Moho depth of more than 10 km is observed at the transition. Seismic velocities at the transition are the highest observed (>7.2 km s^{-1}) along the entire continental section. We attribute this to magmatic intrusions during the early break-up process in the Fram strait.

(iv) The oceanic crust adjacent to the continent–ocean transition is thin, ranging between 2 and 4 km. This thickness is in contrast to earlier published work, specifically Czuba *et al.* (1999). The observed seismic velocities indicate the absence of oceanic layer 3. We attribute the thinning to decreased partial melting to conductive heat loss at the (slow-spreading) Molloy and Knipovich Ridges. Sedimentary sequences more than 4 km thick are observed in the Molloy Ridge crustal segment, compared with only 2 km in the Knipovich Ridge segment. Differential loading possibly lead to a hinge-like behaviour and normal faulting at of the Molloy Transform Fault

(v) The occurrence of a transform margin off Kongsfjorden directly adjacent to a rifted segment ∼100 km further south (Ritzmann 2003), leads to the assumption that the western margin of Svalbard is segmented similarly to the Barents sea margin further south.

ACKNOWLEDGMENTS

The authors sincerely thank the captains and crews of RV Polarstern and El Tanin, and gratefully acknowledge the participation of P. Sroda who supported the experiment realization during the cruise. Additional thanks is given to T. Boebel who performed the basic processing on airborne gravity data used for central Svalbard.

REFERENCES

Amundsen, H.E.F., Griffin, W.L. & O'Reilly, S.Y., 1987. The lower crust and upper mantle beneath northwestern Spitsbergen: evidence from xenoliths and geophysics, *Tectonophysics,* **139,** 169–185.

Austegard, A. & Sundvor, E., 1991. The Svalbard continental margin: Crustal structure from analysis of deep seismic profiles and gravity, *Seismo-Series* 53, University of Bergen, Bergenp, p. 31.

Baturin, D.G., 1990. Structure and Geodynamics of the Malloy Transform Fault Zone in the Mid-Oceanic Ridge System of the Norway-Greenland Basin, *Oceanology,* **30,** 316–320.

Boebel, T., 2000. Airborne topography and gravimetry: System and application to Fram Strait, Svalbard and Northeast Greenland, *Reports on Polar Research*, Vol. 366, Alfred Wegener Institute for Polar and Marine Research, Bremerhaven, p. 366.

Bown, J.W. & White, R.S., 1994. Variation with spreading rate of oceanic crustal thickness and geochemistry, *Earth. planet. Sci. Lett.,* **121,** 435–449.

Breivik, A.J., Verhoef, J. & Faleide, J.I., 1999. Effect of thermal constraints on gravity modeling at passive margins: Results from the western Barents Sea, *J. geophys. Res.,* **104,** 15 293–15 311.

Breivik, A.J., Mjelde, R., Grogan, P., Shimamura, H., Murai, Y. & Nishimura, Y., 2003. Crustal structure and transform margin development south of Svalbard based on ocean bottom seismometer data, *Tectonophysics,* **369,** 37–70.

Chan, W.W. & Mitchell, B.J., 1982. Synthetic seismogram and surface wave contrains on crustal models of Spitsbergen, *Tectonophysics,* **89,** 51–76.

Christensen, N.I., 1966. The elasticity of ultrabasic rocks, *J. geophys. Res.,* **71,** 5921–5931.

Christensen, N.I., 1978. Ophiolites, seismic velocities, and ocean crustal structure, *Tectonophysics,* **47,** 131–157.

Christensen, N.I. & Mooney, W.D., 1995. Seismic velocity structure and composition of the continental crust: A global view, *J. geophys. Res.,* **100(B7),** 9761–9788.

Crane, K., Sundvor, E., Buck, R. & Martinez, F., 1991. Rifting in the Northern Norwegian-Greenland sea: Thermal Tests of Asymmetric Spreading, *J. geophys. Res.,* **96(B9),** 14 529–14 550.

Crane, K., Doss, H., Vogt, P., Sundvor, E., Cherkashov, G., Poroshima, I. & Joseph, D., 2001. The role of the Spitsbergen sher zone in determining morphology, segmentation and evolution of the Knipovich Ridge, *Mar. Geophys. Res.,* **22,** 153–205.

Czuba, W., Grad, M. & Guterch, A., 1999. Crustal structure of north-western Spitsbergen from DSS measurements, *Polish Polar Research,* **20,** 131–148.

Dallmann, W.K., Andersen, A., Bergh, S.G., Maher, H.D., Jr, Jr & Ohta, Y., 1993. Tertiary fold-and-thrust belt of Spitsbergen Svalbard, *Norsk Polarinstitutt Meddelelser,* **128,** 5–46.

Detrick, R.S., White, R.S. & Purdy, G.M., 1993. Crustal structure of North Atlantic Fracture Zones, *Rev. Geophys.,* **31,** 439–458.

Edwards, R.A., Whitmarsh, R.B. & Scrutton, R.A., 1997. The crustal structure across the transform continental margin off Ghana, eastern equatorial Atlantic, *J. geophys. Res.,* **102,** 747–772.

Eiken, O., 1993. An outline of the northwestern Svalbard continenal margin, in *Arctic Petroleum Potential*, NPF Special Publication **2,** 619–629, eds Vorren, T.O., Bergsager, E., Dahl-Stamnes, Ø.A., et al Elsevier, Amsterdam.

Eiken, O., 1994. Seismic Atlas of Western Svalbard—A selection of regional seismic transects, *Norsk Polarinstitutt Meddelelser,* **130,** 3–73.

Eiken, O. & Austegard, A., 1987. The Tertiary orogenic belt of West-Spitsbergen: Seismic expressions of the offshore sedimentary basins, *Norsk Geologisk Tidsskrift,* **67,** 383–394.

Eiken, O. & Hinz, K., 1993. Contourites in the Fram Strait, *Sed. Geol.,* **92,** 15–32.

Eldholm, O., Faleide, J.I., & Myhre, A.M., 1987. Continent-ocean transition at the western Barents Sea/Svalbard continental margin, *Geology,* **15,** 1118–1122.

Eldholm, O., Karasik, A.M. & Reksnes, P.A., 1990. The North American plate boundary, in, *The Arctic Ocean region, Band L of The Geology of North America*, pp. 171–184, eds Grantz, A., Johnson, L. & Sweeney, J.F., Geological Society of America, Boulder, Colorado.

Faleide, J.I., Gudlaugsson, S.T., Eldholm, O., Myhre, A.M. & Jackson, H.R., 1991. Deep seismic transects across the sheared western Barents Sea-Svalbard continental margin, *Tectonophysics,* **189,** 73–89.

Friend, P.F., Harland, W.B., Rogers, D.A., Snape, I. & Thorney, S., 1997. Late Silurian and Early Devonian stratigraphy and probable strike-slip tectonism in north-western Spitsbergen, *Geol. Mag.,* **134,** 459–479.

Geissler, W. H., 2001. Marine seismische Untersuchungen am nördlichen Kontinentalrand von Svalbard (Spitzbergen)., *unpublished diploma thesis*, Institut für Geophysik der Technischen Universität Bergakademie Freiberg, Freiberg.

Guterch, A., Pajchel, J., Perchuc, E., Kowalski, J., Duda, S., Komber, G., Bojdys G. & Sellevoll, M.A., 1978. *Seismic reconnaissance measurements on the crustal structure in the Spitsbergen Region 1976*, University of Bergen Seismological Observatory, Bergen.

Håkansson, E. & Pedersen, S.A.S., 1982. Late Paleozoic to Tertiary tectonic evolution of the continental margin in North Greeland, in, *Arctic Geology and Geophysics*, Can. Soc. Pet. Geol. Mem. 8, pp. 331–348, eds Embry, A.F. & Balkwill, H.R. Canadian Society of Petroleum Geologists, Calgary.

Hajnal, Z., Burianyk, M.J.A., Kesmarky, I., & Overton, A., 1990. Reflection Survey on Hobson's Choise Island, Arctic Ocean, *Marine Geology,* **93,** 211–224.

Harland, W.B. & Wright, N.J.R., 1979. Alternative hypothesis for the pre-Carboniferous evolution of Svalbard., *Norsk Polarinstitutt Skrifter,* **167,** 89–117.

Harland, W.B., 1997a. Svalbard's geological frame, in, *The Geology of Svalbard*, pp. 23–44, Geological Survey Memoir 17, ed. Harland, W.B. The Geological Society London, UK.

Harland, W.B., 1997b. Devonian History, in, *The Geology of Svalbard*, Geological Survey Memoir 17, pp. 289–309, ed. Harland, W.B. The Geological Society London, UK.

Harland, W.B., 1997. Central Western Spitsbergen (with a contribution with Geddes, I. & Doubleday, P.A.), in, *The Geology of Svalbard*, Geological Survey Memoir 17, ed. Harland, W.B. The Geological Society London, UK.

Hjelle, A. & Lauritzen, Ø., 1982. *Geological Map of Svalbard 1 : 500 000 Sheet 3G*, Spitsbergen northern part, Norsk Polarinstitutt, Oslo.

Howells, K., Masson Smith, D. & Maton, P.I., 1977. Some rock and formation densities from Svalbard, *Norsk Polarinstitutt rbok,* **1975,** 53–67.

Horn, J.R., Clowes, R.M., Ellis, R.M. & Bird, D.N, 1984. The seismic structure across an active oceanic/continental transform fault zone, *J. geophys. Res.,* **89,** 3107–3120.

Jackson, H.R., 1990. Evolution and Regional Stratigraphy of the Northeastern Canadian Polar Margin, *Mar. Geol.,* **93,** 179–192.

Jakobsson, M., Cherkis, N.Z., Woodward, J., Macnab, R. & Coakley, 2000. New grid of Arctic bathymetry aids scientists and mapmakers, *EOS, Trans. Am. geophys. Un.,* **81**, 89, 93, and 96.

Jokat, W. et al, 2000. Marine Geophysics, in, *The Expedition ARKTIS-XV/2 of 'Polarstern' in 1999*, Reports on Polar Research 368, pp. 8–26, ed. Jokat, W. Alfred Wegener Institute for Polar and Marine Research, Bremerhaven.

Jokat, W. *et al.*, 2003. Geophysical Investigations, in, *The Expedition ARKTIS XVIII/2 of RV Polarstern in 2002 Contributions of the Participants*, Reports on Polar Research 449, pp. 8–32, ed. Jokat, W. Alfred Wegener Institute for Polar and Marine Research, Bremerhaven.

Klingelhöfer, F., Géli, L., Matias, L., Steinsland, N., Mohr, J., 2000. Crustal structure of a super-slow spreading centre: a seismic refraction study of Mohns Ridge, 72°N, *Geophys. J. Int.,* **141,** 509–526.

Kurinin, R.G., 1970. Density and Magnetic Suscpetibilities of Spitsbergen Rocks, in, *Geology of Spitsbergen (1965)* **2**, pp. 284–286, ed. Harland, W.B. National Lending Library for Science and Technology, Yorshire, UK.

Lepvrier, C. & Geyssant, 1985. L'evolution structurale de la marge occidentale du Spitsberg: coulissement et rifting tertiares, *Bulletin de la Société Géologique du Nord,* **103,** 333–344.

Lorenzo, J.M. *et al.*, 1991. Development of the continent-ocean transform boundary of the southern Exmouth Plateau, *Geology,* **19,** 843–846.

Lorenzo, J.M., 1997. Sheared continent-ocean margins: an overview, *Geo-Marine Lett.,* **17,** 1–3.

Lowell, J.D., 1972. Spitsbergen Tertiary Orogenic Belt and the Spitsbergen Fracture Zone, *Geol. Soc. Am. Bul.,* **83,** 3091–3102.

Manby, G. & Lyberis, N., 1992. Tectonic evolution of the Devonian Basin of northern Svalbard, in, *Post-Caledonian Tectonic Evolution of Svalbard*, Norsk Geologisk Tidsskrift 72, pp. 7–19, eds Dallmann, W.K., Andresen, A. & Krill, A. Scandinavian University Press, Oslo.

Minshull, T.A., Muller, M.R., Robinson, C.J., White, R.S. & Bickle, M.J., 1998. Is the oceanic Moho a serpentinization front?, in, *Modern Ocean Floor Processes and the Geological Record*, Geol. Soc. Spec. Pub. 148, pp. 71–80, eds. Mills, R.A. & Harrison, K. The Geological Society of London, London.

Mooney, W.D. & Meissner, R., 1992. Multi-genetic origin of crustal reflectivity: continental lower crust and Moho, in, *Continental Lower Crust*, Developments in Geotectonics 23, pp. 45–78, eds Foutain, D.M., Arculus, R. & Kay, R.W. Elsevier, Amsterdam.

Mutter, J.C., Buck, W.R. & Zehnder, C.M., 1988. Convective partial melting 1. A model for the formation of thick basaltic sequences during the initation of spreading, *J. geophys. Res.,* **93,** 1031–1048.

Myhre, A.M., Eldholm, O. & Sundvor, E., 1982. The margin between Senja and Spitsbergen fracture zones: Implications from plate tectonics, *Tectonophysics,* **89,** 1–32.

Myhre, A. M., & Eldholm, O., 1988. The Western Svalbard margin (74°–80°N)., *Marine and Petroleum Geol.,* **5,** 143–156.

Okay, N. & Crane, K., 1993. Thermal Rejuvenation of the Yermak Plateau., *Mar. Geophys. Res.,* **15,** 243–263.

Reid, I.D., 1988. Crustal structure beneath the southern Grand Banks: seismic-refraction results and their implications., *Can. J. Earth Sci.,* **25,** 760–772.

Reid, I.D. & Jackson, H.R., 1981. Oceanic spreading rate and crustal thickness., *Mar. Geophys. Res.,* **5,** 165–172.

Reid, I.D. & Jackson, H.R., 1997. A review of three transform margins off eastern Canada., *Geo-Marine Lett.,* **17,** 87–93.

Ritzmann, O., 2003. Architecture and geodynamic evolution of the Svalbard Archipelago, the Yermak Plateau and the Fram Strait oceanic province, from deep seismic experiments, *Reports on Polar Research*, **439**, Alfred Wegener Institute for Polar and Marine Research, Bremerhaven.

Ritzmann, O. & Jokat, W., 2003. Crustal structure of northwestern Svalbard and the adjacent Yermak Plateau: Evidence for Oligocene detachment tectonics and non-volcanic break-up., *Geophys. J. Int.,* **152,** 139–159.

Ritzmann, O., Jokat, W., Mjelde, R., Shimamura, H., 2002. Crustal structure between the Knipovich Ridge and the Van Mijenfjorden (Svalbard), *Mar. Geophys. Res.,* 23(5), in press.

Schlindwein, V. & Jokat, W., 1999. Structure and evolution of the continental crust of northern east Greenland from integrated geophysical studies., *J. geophys Res.,* **104,** 15 227–15 245.

Sellevoll, M.A., Duda, S.J., Guterch, A., Pajchel, J., Perchus, E. & Thyssen, F., 1991. Crustal structure in the Svalbard region from seismic measurements., *Tectonophysics,* **189,** 55–71.

Srivastava, S.P. & Tapscott, C.R., 1986. Plate kinematics of the North Atlantic, in, *The Western North Atlantic Region*, The Geology of North America M, pp. 379–404, eds Vogt, P.R. & Tucholke, B.E. Geological Society of America, Boulder.

Steel, R.J., Helland-Hansen, W., Kleinspehn, K., Nøttvedt, A. & Rye-Larsen, M., 1985. The Teriary strike-slip basins and orogenic belt of Spitsbergen, in, *Strike-slip deformation, Basin formation and Sedimentation*, Special Publications Society of Economic Paleontologists and Mineralogists 37, pp. 339–359, eds Biddle, K.T. & Christie-Blick, N. Publisher SEPM Society for Sedimentary Geology, Tulsa.

Sundvor, E. & Austegard, A., 1990. The Evolution of the Svalbard Margins: Synthesis and new Results, in, *Geological History of the Polar Oceans: Arctic Versus Antarctic*, pp. 77–94, eds Bleil, U. & Thiede, J. Kluwer Academic Publishers, Dordrecht.

Talwani, M. & Eldholm, O., 1977. Evolution of the Norwegian-Greenland Sea, *Geol. Soc. Am. Bul.,* **88,** 969–999.

Todd, B.J., Reid, I.D. & Keen, C.E., 1988. Crustal structure across the southwest Newfoundland transform margins, *Can. J. Earth Sci.,* **25,** 744–759.

Verhoef, J., Roest, W.R., Macnab, R., Arkani-Hamed, & members of the project team, 1996. *Magnetic anomalies of the Arctic and North Atlantic Oceans and adjacent land areas*, GSC Open file 3125, Geological Survey of Canada Dartmouth, Nova Scotia.

White, R.S., McKenzie, D. & O'Nions, R.K., 1992. Oceanic Crustal Thickness From Seismic Measurements and Rare Earth Element Inversions, *J. geophys. Res.,* **97,** 19 683–19 715.

White, R.S., Minshull, T.A., Bickle, M.J. & Robinson, C.J., 2001. Melt generation at very slow-spreading oceanic ridges; constraint from geochemical and geophysical datatit J. Petrol., **42,** 1171–1196.

Zelt, C.A. & Smith, R.B., 1992. Seismic travel time inversion for 2-D crustal velocity structure, *Geophys. J. Int.,* **108,** 16–34.